Parton Energy Loss and Modified Beam Quark Distribution Functions in Drell-Yan Process in $p + A$ Collisions

Hongxi Xing[a,b], Yun Guo[c,d], Enke Wang[a] and Xin-Nian Wang[a,b]

[a] *Institute of Particle Physics, Central China Normal University, Wuhan 430079, China*
[b] *Nuclear Science Division, MS 70R0319,*
Lawrence Berkeley National Laboratory, Berkeley, CA 94720
[c] *Department of Physics, Guangxi Normal University, Guilin 541004, China*
[d] *Department of Physics, Brandon University,*
Brandon, Manitoba, R7A 6A9 Canada

Abstract

Within the framework of generalized collinear factorization in perturbative QCD (pQCD), we study the effect of initial multiple parton scattering and induced parton energy loss in Drell-Yan (DY) process in proton-nucleus collisions. We express the contribution from multiple parton scattering and induced gluon radiation to the DY dilepton spectra in terms of nuclear modified effective beam quark distribution functions. The modification depends on the quark transport parameter in nuclear medium. This is similar to the final-state multiple parton scattering in deeply inelastic scattering (DIS) off large nuclei and leads to the suppression of the Drell-Yan cross section in $p + A$ relative to $p + p$ collisions. With the value of quark transport parameter determined from the nuclear modification of single-inclusive DIS hadron spectra as measured by the HERMES experiment, we calculate DY spectra in $p + A$ collisions and find the nuclear suppression due to beam parton energy loss negligible at the Fermilab energy $E_{\rm lab}$=800 GeV in the kinematic region as covered by the E866 experiment. Most of the observed nuclear suppression of DY spectra in E866 experiment can be described well by parton shadowing in target nuclei as given by the EPS08 parameterization. The effect of beam parton energy loss, however, becomes significant for DY lepton pairs with large beam parton momentum fraction x' or small target parton momentum fraction x. We also predict the DY cross section in $p + A$ collisions at lower beam proton energy $E_{\rm lab}$=120 GeV and show significant suppression due to initial state parton energy loss at moderately large x' where the effect of parton shadowing is very small.

I. INTRODUCTION

A basic assumption in the collinear factorized parton model in perturbative QCD (pQCD) is the small intrinsic transverse momentum of initial partons inside beam hadrons or nuclei relative to both partons' longitudinal momenta and the large energy-momentum scale Q involved in hard partonic interactions. To go beyond such a collinear factorized pQCD model, one has to expand the hard partonic part of the hard interaction in the intrinsic parton transverse momentum. In such an expansion, the first term gives rise to the normal collinear factorized pQCD results, known as the leading twist contributions which will depend on leading twist transverse-momentum-integrated parton distribution functions. The higher order terms in the Taylor expansion can be combined together with contributions from multiple parton interaction between incoming or out-going partons and the remanent of target hadrons/nuclei. These contributions are known as higher twist contributions which can be expressed as the convolution of hard parts involving multiple parton scattering and multiple parton correlation functions inside the target hadrons/nuclei in the framework known as generalized collinear parton model [1, 2]. These higher-twist contributions in general are suppressed by powers of the momentum scale in the hard processes, $1/Q^n$.

In hard processes involving a large nuclear target, higher-twist contributions often depend on multiple parton correlation functions inside the target nucleus which are enhanced by the nuclear size $R_A \sim A^{1/3}$ [3–5]. These will give rise to a leading and non-trivial nuclear dependance of the higher-twist contributions to the hard processes beyond the incoherent superposition of nucleons inside a nucleus. One example of such nuclear enhanced higher-twist contributions is the suppression of leading hadron spectra in deeply inelastic scattering (DIS) off a nucleus relative to that in DIS off a nucleon and the suppression is observed to increase with the nuclear size as in the HERMES experiment [6]. Such a suppression has been studied within the generalized collinear parton model [7–9] and was shown to be caused by multiple parton scattering of the struck quark and induced gluon radiation inside the target nucleus. The gluon radiation induced by multiple parton scattering that reduces the energy of the propagating quark can be expressed as a nuclear modification to the effective fragmentation function of the struck quark [7], which is determined by the quark-gluon correlation function inside the nucleus, a higher twist matrix element of the nucleus not calculable in pQCD. Assuming a large and loosely bound nucleus, one can approximate these higher twist matrix elements as a product of initial quark distribution and gluon density distribution inside the nucleus, the latter is also known as the quark transport parameter inside the nuclear medium [4]. The parton transport parameter also describes the medium broadening of transverse momentum squared [10, 11] per unit distance and is equivalent to the saturation scale per unit length in a large nucleus [12, 13]. One can determine this quark transport parameter by comparing the leading hadron spectra suppression in DIS off a nuclear target to experimental data. The predicted nuclear size and quark energy dependence of the hadron suppression agree very well with the experiment [14, 15].

One can further extend the study of medium modification of parton fragmentation functions and parton energy loss or jet quenching due to multiple parton scattering and induced gluon radiation to the case of parton propagation inside a hot quark-gluon plasma (QGP) in heavy-ion collisions. In this case one has to replace the cold nuclei with a hot thermal medium of quarks and gluons [5, 14, 16]. The parton transport parameter is then proportional to gluon distribution density inside the hot QGP. Therefore the study of jet quenching

in high-energy heavy-ion collisions can provide crucial information of space-time profile of parton density distribution in the early stage of heavy-ion collisions [17]. The observed suppression of single [18, 19], dihadron spectra [20] and gamma-hadron correlation [21, 22] in high-energy heavy-ion collisions at RHIC are all consequences of strong jet quenching and provided the evidence for the formation of a strongly coupled QGP in the center of heavy-ion collisions at RHIC [23, 24]. Recent data from heavy-ion collisions at the LHC [25] have also shown a wide range of phenomena of jet quenching which point to the formation of a strongly coupled QGP similar to that formed in heavy-ion collisions at RHIC.

Multiple scattering and induced parton energy loss have been studied in several theoretical frameworks [26–29], among which the higher-twist approach can be applied to jet propagation in both hot QGP and cold nuclei. In high-energy heavy-ion collisions, energetic partons which one uses as hard probes have to traverse not only the hot QGP in the early stage of the dense matter but also hadronic medium after hadronization of the QGP matter. One therefore has to include the effect of jet quenching due to multiple parton scattering during the hadronic phase of the dense matter evolution in high-energy heavy-ion collisions. Using the information of parton energy loss in cold nuclei in DIS off large nuclei and extrapolate to hadronic medium at finite temperature, a recent study [30] finds non-negligible contribution from jet quenching in hadronic phase to the final suppression of large p_T hadron spectra in heavy-ion collisions at RHIC and LHC. Therefore, the study and inclusion of parton energy loss in cold nuclei and hadronic matter should be an integral part of phenomenological study of jet quenching in heavy-ion collisions.

In this paper, we will study the effect of multiple parton scattering and parton energy loss in the Drell-Yan (DY) process of dilepton production in $p+A$ collisions. Since dilepton pairs in the final state do not have strong interaction with the target nucleus, only initial state interactions are important in DY process. Therefore, it is an ideal tool to study fast parton propagation and energy loss in cold nuclear medium [31–37]. The higher-twist approach has also been applied to the study of nuclear effects in the DY process in $p+A$ collisions [38, 39]. These studies were restricted to the large transverse momentum DY pairs, where one can neglect the interferences associated with induced gluon radiation. In the calculation of the total DY cross section, one has to integrate over the transverse momentum of the DY pairs and therefore has to take into account of the interferences.

Our approach to the nuclear effects in DY pair production in $p+A$ collisions is very similar to the study of nuclear modification of the effective fragmentation functions in DIS. Initial multiple parton scattering and induced gluon radiation before the DY pair production via quark-anti-quark annihilation can lead to parton energy loss and attenuation of the incoming beam partons. In the collinear approximation, transverse momentum of the initial partons are neglected. The transverse momentum of the final DY pairs is then determined by the transverse momentum of the radiated gluon either in the vacuum or medium induced gluon bremsstrahlung. In the process involving multiple parton scattering, there are destructive interferences between the amplitudes of vacuum gluon bremsstrahlung and gluon radiation induced by multiple scattering. It is often referred to as the Landau-Pomercanchuk-Migdal (LPM) interference [40]. The LPM interference effect can be characterized by the formation time of the radiated gluon which is inversely proportional to the transverse momentum squared q_T^2. For large q_T^2 or short formation time, interference between vacuum and medium induced gluon bremsstrahlung is negligible. However, for small q_T^2, the gluon formation time becomes longer than or comparable to the nuclear size and there is strong destructive interference between vacuum and medium induced gluon bremsstrahlung that cancels the

effect of gluon radiation due to multiple parton scattering. In our study of DY pair spectra, we will include explicitly the LPM interference within the framework higher-twist approach.

Similar to the parton energy loss and medium modification of the effective parton fragmentation functions in DIS, we can express the nuclear effect in the DY process due to the initial multiple parton scattering and induced parton energy loss by the beam parton in terms of modified beam parton distribution functions. The medium modification can be effectively included in terms of the modified splitting functions in the QCD evolution equations which depend on twist-4 quark-gluon correlation functions inside the nucleus. With the approximation that the quark-gluon parton correlation can be factorized as a product of the quark and gluon distribution, the medium modified splitting functions depend only on the parton transport parameter $\hat{q}$, which is related to the distribution density of soft gluons inside the nucleus or the broadening of transverse momentum squared per unit length due to multiple scattering. This is the only free parameter in the higher-twist study in both DIS and DY process with a nucleus target. One therefore can use the information from the phenomenological study of hadron suppression in DIS experiment [15] and calculate the nuclear suppression due to parton energy loss in the DY process [41].

Coherence in multiple scattering between beam and target partons can also lead to the nuclear shadowing of parton distributions inside the target nucleus. This and other nuclear modifications of the parton distributions has been measured in nuclear DIS [42] and parametrized [43, 44] from global fitting of experimental data involving nuclear targets. These nuclear modifications of parton distributions can also lead to nuclear effects in DY spectra in $p+A$ versus that in $p+p$ collisions. We will use the EPS08 parameterization [43] of the nuclear parton distribution functions (nPDF) for the target nucleus in the calculation of DY spectra in addition to the effect of parton energy loss and medium modification of the beam parton distributions. We will then compare the calculated DY spectra to the data from the Fermilab Experiment 866 (E866) [32]. We will compare the effect of nuclear shadowing of target partons and the beam parton energy loss and investigate in which kinetic region the effect of beam parton energy loss dominate.

The remainder of the paper is organized as the following. In Sec. II, we define our notations and discuss the leading twist processes and the vacuum Dokshitzer-Gribov-Lipatov-Altarelli-Parisi (DGLAP) evolution [45, 46] of parton distribution functions. In Sec. III, we calculate the twist-4 contribution to DY cross section within the framework of generalized factorization. We then define the effective modified beam quark distribution functions in Sec. IV and discuss the energy loss effect on the DY cross section. We summarize our results in Sec. V. The complete results of the twist-4 annihilation-like and Compton-like processes are given in the Appendix A and B, respectively. We also demonstrate that the twist-4 contributions from double-hard scattering can be understood as the successive single scatterings in Appendix C.

II. LEADING TWIST CONTRIBUTIONS

In this paper, we focus on the production of DY lepton pairs in unpolarized $h+A$ collisions,

$$h(p') + A(p) \to \begin{array}{l} \gamma^*(q) + X, \\ \hookrightarrow l^+ l^- \end{array} \tag{1}$$

whose cross section can be expressed in terms of the virtual photon $\gamma^*(q)$ production cross section,

$$\frac{d\sigma_{hA\to l^+l^-}}{d^4q} = \frac{2\alpha_{em}}{3Q^2}\frac{d\sigma_{hA\to\gamma^*}}{d^4q}. \tag{2}$$

Here p' is the four-momentum of the incoming beam hadron, p is the momentum per nucleon inside the target nucleus and q is the four-momentum of the DY lepton pair. In the center-of-mass frame, we can choose the nucleus and the beam hadron moving along the "plus" and "minus" direction, respectively. Using light-cone notations, the momenta of beam hadron, target nucleus and virtual photon can be expressed as

$$p' = [0, p'^-, \vec{0}_\perp], \qquad p = [p^+, 0, \vec{0}_\perp], \qquad q = [(Q^2+q_T^2)/2q^-, q^-, \vec{q}_T], \tag{3}$$

where the "plus" and "minus" components are defined as $p^\pm = (p_0 \pm p_z)/\sqrt{2}$.

According to the collinear factorization [47], the Drell-Yan cross section in $h+A$ collisions can be expressed,

$$\frac{d\sigma_{hA\to\gamma^*}}{d^4q} = \sum_c \int dx' f_{c/h}(x')\frac{d\sigma_{cA\to\gamma^*}}{d^4q} \equiv \int dx' \frac{d\sigma_{hA\to\gamma^*}}{d^4q dx'}, \tag{4}$$

in terms of the product of parton(c)-nucleus cross section $d\sigma_{cA\to\gamma^*}$ and the normal twist-two beam parton distribution function $f_{c/h}(x')$, where $x' = q^-/p'^-$ is the momentum fraction carried by the annihilated beam quark.

Inside the nuclear target, the beam parton may undergo additional scattering before the production of the lepton pair. Within the framework of twist expansion, one can calculate the contribution to the parton-nucleus cross section as a sum of contributions from single scattering, double scattering and even higher multiple scattering

$$\frac{d\sigma_{cA\to\gamma^*}}{d^4q} = \frac{d\sigma^S_{cA\to\gamma^*}}{d^4q} + \frac{d\sigma^D_{cA\to\gamma^*}}{d^4q} + \dots . \tag{5}$$

We will calculate contributions up to double scatterings in this paper.

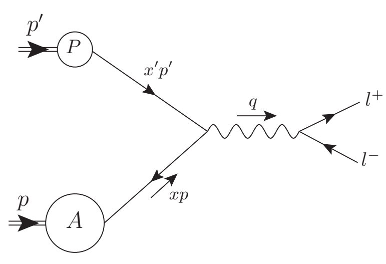

FIG. 1: Lowest order Drell-Yan process at leading twist.

The leading-twist contribution to DY dilepton pair production at the lowest order $\mathcal{O}(\alpha_s^0)$ comes from the quark anti-quark annihilation process as illustrated in Fig. 1. The corresponding differential cross section is given by [48]

$$\frac{d\sigma^{S(0)}_{hA\to\gamma^*}}{dQ^2dx'} = \sum_q \int dx f_{\bar{q}/A}(x) f_{q/h}(x') H_0(x, p, q)\,, \tag{6}$$

where the summation is over all possible quark and anti-quark and $f_{\bar{q}/A}(x)$ denotes the anti-quark (quark) distribution function in the nucleus with momentum fraction x and the hard part of quark anti-quark annihilation is

$$H_0(x,p,q) = \frac{2\pi\alpha_{em}e_q^2}{3x's}\delta(x-x_B). \tag{7}$$

Here $x_B = Q^2/2p\cdot q$ is the Bjorken variable in the DY process, $s=(p+p')^2$ is the center-of-mass energy per $h+N$ collision.

To consider the scale dependence of beam quark distribution function, one has to consider radiative corrections to the annihilation processes and Compton scattering process as illustrated in Fig. 2. In the annihilation process, the beam quark can radiate a gluon before its annihilation with the anti-quark from the target as illustrated in Fig. 2(a) and (b). The annihilating beam quark can also be generated from a beam gluon splitting as shown in Fig. 2(c) which is actually a Compton scattering process.

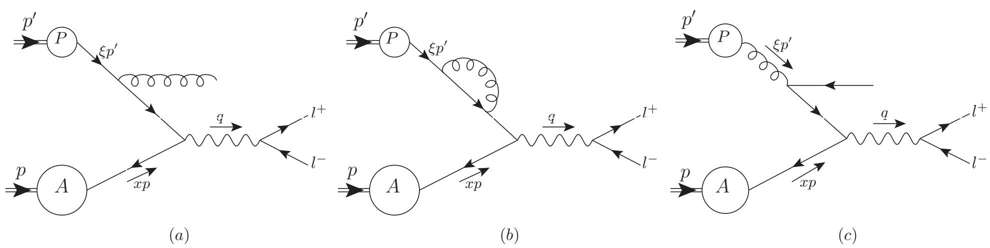

FIG. 2: Next-to-leading order Drell-Yan annihilation process (a,b) and compton scattering (c) at leading twist.

After including the radiative contributions in Fig. 2 with the leading logarithmic approximation (for q_T^2 up to a factorization scale μ^2), the renormalized beam quark distribution can be defined as

$$\begin{aligned} f_{q/h}(x',\mu^2) &= f_{q/h}(x') + \frac{\alpha_s}{2\pi}\int_0^{\mu^2}\frac{dq_T^2}{q_T^2}\int_{x'}^1\frac{d\xi}{\xi}\Big[f_{q/h}(\xi)\gamma_{q\to qg}(x'/\xi) \\ &+ f_{g/h}(\xi)\gamma_{g\to q\bar{q}}(x'/\xi)\Big]. \end{aligned} \tag{8}$$

The first and second term inside the square brackets represent contributions from the annihilation and Compton processes, respectively. The corresponding quark and gluon splitting functions are given by

$$\gamma_{q\to qg}(z) = C_F\left[\frac{1+z^2}{(1-z)_+}+\frac{3}{2}\delta(1-z)\right], \tag{9}$$

and

$$\gamma_{g\to q\bar{q}}(z) = T_R\left[z^2+(1-z)^2\right], \tag{10}$$

where $C_F=4/3$ and $T_R=1/2$ are the color factors.

The renormalized quark distribution function satisfies the vacuum DGLAP evolution equation,

$$\frac{\partial f_{q/h}(x',\mu^2)}{\partial \ln\mu^2} = \frac{\alpha_s}{2\pi}\int_{x'}^{1}\frac{d\xi}{\xi}\left[f_{q/h}(\xi,\mu^2)\gamma_{q\to qg}(x'/\xi)+f_{g/h}(\xi,\mu^2)\gamma_{g\to q\bar{q}}(x'/\xi)\right]. \tag{11}$$

Similarly, one can also obtain the renormalized target quark distribution function and its vacuum DGLAP evolution equations.

III. TWIST-FOUR CONTRIBUTION

When a parton is passing through nuclear matter, it will suffer multiple scattering and parton energy loss. In principle, contributions from multiple scattering are power-suppressed for large invariant mass $M=Q$ or transverse momentum q_T of the DY lepton pair. However, if the involved target partons in multiple scattering come from different nucleons inside the nucleus, some contributions can be enhanced by the nuclear size $A^{1/3}$ for each additional scattering. In this paper, we consider twist-4 contributions which are enhanced by the nuclear medium size. We will only consider the case of secondary scattering with another target gluon because the involved gluon-quark correlation in the nucleus is believed to be much larger than quark-quark correlation in the double quark rescattering [49].

A. Factorization

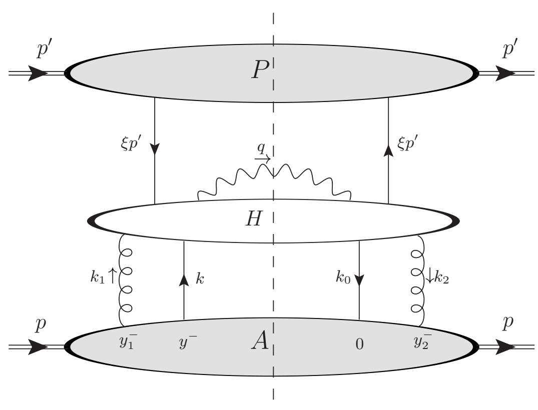

FIG. 3: Next-to-leading order Drell-Yan annihilation process at twist-four.

In the covariant gauge, the double scattering as shown in Fig. 3 in general can be cast in the following factorized form:

$$\begin{aligned}\frac{d\sigma^D_{qA\to\gamma^*}}{d^4q} &= \frac{1}{2\xi s}\int d^2k_T\int\frac{dy^-}{2\pi}\frac{dy_1^-}{2\pi}\frac{dy_2^-}{2\pi}\frac{d^2y_T}{(2\pi)^2}e^{-i\vec{k}_T\cdot\vec{y}_T}\overline{H}(y^-,y_1^-,y_2^-,k_T,p,q)\\ &\times\frac{1}{2}\langle A|A^+(y_2^-,0_T)\bar{\psi}_q(0)\gamma^+\psi_q(y^-)A^+(y_1^-,y_T)|A\rangle,\end{aligned} \tag{12}$$

where $k_0=[(x+x_2)p^+,0,\vec{0}_\perp]$, $k=[xp^+,0,\vec{0}_\perp]$, and we keep for now the relative intrinsic transverse momentum k_T carried by target gluon with $k_1=[x_1p^+,0,\vec{k}_T]$ and $k_2=[(x_1-$

$x_2)p^+, 0, \vec{k}_T]$. $\overline{H}$ is the Fourier transform of the hard part $\widetilde{H}$ in momentum space,

$$\overline{H}(y^-, y_1^-, y_2^-, k_T, p, q) = \int dx dx_1 dx_2 e^{ixp^+y^-} e^{ix_1p^+y_1^-} e^{-i(x_1-x_2)p^+y_2^-} \times \widetilde{H}(\xi, x, x_1, x_2, k_T, p', p, q). \quad (13)$$

As part of the twist expansion, one makes a Taylor expansion of the partonic part $\overline{H}$ in the gluon's intrinsic transverse momentum around $k_T = 0$ [50]:

$$\overline{H}(y^-, y_1^-, y_2^-, k_T, p, q) = \overline{H}(y^-, y_1^-, y_2^-, k_T = 0, p, q) + \left.\frac{\partial \overline{H}}{\partial k_T^\alpha}\right|_{k_T=0} k_T^\alpha + \frac{1}{2} \left.\frac{\partial^2 \overline{H}}{\partial k_T^\alpha \partial k_T^\beta}\right|_{k_T=0} k_T^\alpha k_T^\beta + \dots . \quad (14)$$

The first term on the right-hand side of the above equation can be included in the leading-twist eikonal contribution as the gauge link, which makes twist-two parton matrix element from the single-scattering gauge invariant. The second term vanishes after integrating over k_T for unpolarized initial and final states. The third term will give a finite contribution to the double-scattering, which, after integrating over d^2k_T, becomes

$$\frac{d\sigma^D_{qA\to\gamma^*}}{d^4q} = \frac{1}{2\xi s} \int \frac{dy^-}{2\pi} \frac{dy_1^-}{2\pi} \frac{dy_2^-}{2\pi} \frac{1}{2} \langle A| F_\alpha^+(y_2^-) \bar{\psi}_q(0) \gamma^+ \psi_q(y^-) F^{+\alpha}(y_1^-) |A\rangle \times (-\frac{1}{2} g^{\alpha\beta}) \left[\frac{1}{2} \frac{\partial^2}{\partial k_T^\alpha \partial k_T^\beta} \overline{H}(y^-, y_1^-, y_2^-, k_T, p, q)\right]_{k_T=0}, \quad (15)$$

where the factor $k_T^\alpha k_T^\beta$ has been converted into spatial derivatives in the the field strength tensor after partial integration.

B. Double scattering: Annihilation-like and compton-like processes

There are two distinctive processes at twist-four which we will consider here. One is the annihilation-like processes as shown in Fig. 4. Before annihilation into a virtual photon, the beam quark may scatter with another gluon from the nucleus. Such multiple parton scattering processes will effectively modify the distribution of the beam quark. In our calculation, we neglect the leading order twist-4 processes because our purpose in this paper is to study the effect of radiative parton energy loss due to the multiple scattering on the beam quark distribution. Without induced gluon radiation, the leading order double scattering mainly contributes to the transverse momentum broadening of the leading parton [51].

As an illustration of the calculation involved, we consider the contribution from the first diagram in Fig. 4. Using the Feynman rules, one can write down the hard part of this diagram

$$\overline{H}_{A11} = \int dx dx_1 dx_2 e^{ixp^+y^-} e^{ix_1p^+y_1^-} e^{-i(x_1-x_2)p^+y_2^-} \frac{1}{2} Tr[\xi \gamma \cdot p' \hat{H}_{A11}] \Gamma^{(2)}, \quad (16)$$

where,

$$\hat{H}_{A11} = \frac{C_F}{2N_c^2} e^2 e_q^2 g^4 \not{p} \frac{\gamma \cdot (\xi p' + k_2)}{(\xi p' + k_2)^2 - i\varepsilon} \gamma^\beta \frac{\gamma \cdot (q - k_0)}{(q - k_0)^2 - i\varepsilon} \gamma^\nu \frac{1}{2} \gamma \cdot p \gamma^\mu \times \frac{\gamma \cdot (q - k)}{(q - k)^2 + i\varepsilon} \gamma^\alpha \frac{\gamma \cdot (\xi p' + k_1)}{(\xi p' + k_1)^2 + i\varepsilon} \not{p} (-g_{\mu\nu}) \varepsilon_{\alpha\beta}(l_g). \quad (17)$$

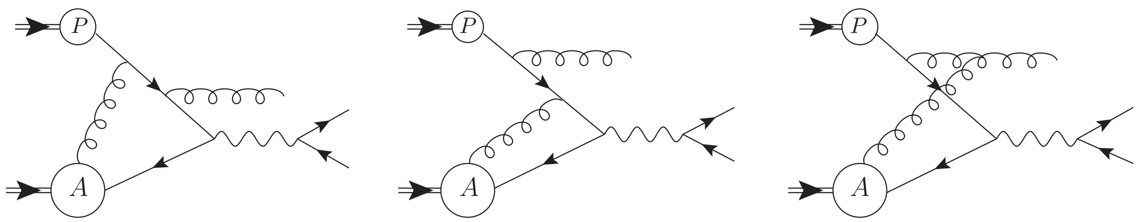

FIG. 4: Next-to-leading order Drell-Yan annihilation process at twist-four.

Throughout this paper, we use the subscript "Aij" to denote different central-cut diagrams at twist-4. We have the following conventions: "A" stands for the annihilation-like processes while "i" and "j" correspond to the i-th and j-th diagrams shown in Fig. 4 which are the left and right side of the cut diagrams, respectively. Similarly, for the Compton-like processes, we use the subscript"Cij" to distinguish different central-cut diagrams.

For central-cut diagrams, the final state phase space is

$$\Gamma^{(2)} = \frac{1}{(2\pi)^3}\frac{x_B}{Q^2}\frac{z}{1-z}\delta(x+x_1-x_B-x_t-x_C). \tag{18}$$

The momentum fractions are defined as

$$x_t = \frac{x_B}{Q^2}\frac{q_T^2}{1-z}, \quad x_C = \frac{x_B}{Q^2}\frac{z(k_T^2-2\vec{q}_T\cdot\vec{k}_T)}{1-z}, \quad x_D = \frac{x_B}{Q^2}zk_T^2. \tag{19}$$

Performing the contour integration $\int dxdx_1dx_2$, the hard part becomes

$$\overline{H}_{A11} = \alpha_{em}e_q^2\alpha_s^2\frac{C_F}{N_c^2}8(2\pi)^2\frac{1+z^2}{1-z}\frac{1}{(\vec{q}_T-z\vec{k}_T)^2}\overline{I}_{A11}, \tag{20}$$

$$\begin{aligned}\overline{I}_{A11} &= \theta(-y_2^-)\theta(y^- - y_1^-)e^{i(x_B+x_t+x_C-x_D)p^+y^-}e^{ix_Dp^+(y_1^- - y_2^-)}\\ &\times \left[1-e^{-i(x_t+x_C-x_D)p^+(y^- - y_1^-)}\right]\left[1-e^{-i(x_t+x_C-x_D)p^+y_2^-}\right].\end{aligned} \tag{21}$$

There are four terms in the above result which correspond to the contributions from four possible physical processes, i.e., soft-hard, double-hard and their interferences. This comes out naturally because of the four possible choices of poles when performing the contour integrations. The interference are destructive in small q_T region, which cancels contributions from soft-hard and double-hard processes. In the limit $q_T \to 0$, there is a complete cancelation among all the processes. This destructive effect is important in our calculation since we are interested in the transverse momentum integrated spectra to which the small angle gluon radiation also contributes.

According to the scheme in the twist expansion, the twist-four contributions comes from the second derivatives of $\overline{H}$ with respect to k_T or the quadratic terms in the Taylor expansion. In general, one can rewrite the quadratic term in collinear expansion as

$$\begin{aligned}\frac{\partial^2\overline{H}}{\partial k_T^\alpha\partial k_T^\beta} \sim &\left[\frac{\partial^2\overline{I}}{\partial x_{k_T}^2}\frac{\partial x_{k_T}}{\partial k_T^\alpha}\frac{\partial x_{k_T}}{\partial k_T^\beta}\right]H + \left[\frac{\partial\overline{I}}{\partial x_{k_T}}\frac{\partial^2 x_{k_T}}{\partial k_T^\alpha\partial k_T^\beta}\right]H + \left[\frac{\partial\overline{I}}{\partial x_{k_T}}\frac{\partial x_{k_T}}{\partial k_T^\alpha}\right]\frac{\partial H}{\partial k_T^\beta}\\ + &\left[\frac{\partial\overline{I}}{\partial x_{k_T}}\frac{\partial x_{k_T}}{\partial k_T^\beta}\right]\frac{\partial H}{\partial k_T^\alpha} + \overline{I}\frac{\partial^2 H}{\partial k_T^\alpha\partial k_T^\beta},\end{aligned} \tag{22}$$

where H is the truncated hard part of the scattering matrix element when $\bar{I}$ that contains all the phase factors is factored out. We denote x_{k_T} the k_T dependent fractional momentum, such as x_C, x_D in Eq. (21). As we will show later, the last term of the above equation that contains second derivative of the truncated hard part H with respect to the intrinsic transverse momentum k_T is proportional to a quark-gluon correlation matrix element. Other terms in the above equations that contain derivatives of the phase factor I will be proportional to the derivative of the quark-gluon matrix elements with respective to the partons' momentum fraction. These terms are also proportional to the power of the momentum fraction $x_t \sim q_T^2/Q^2$ and therefore are suppressed relative to the last term in the above equation for small $q_T^2/Q^2 \ll 1$. This feature is well illustrated by the the second-order derivative of $\overline{H}_{A11}$,

$$-\frac{1}{4}g^{\alpha\beta}\frac{\overline{H}_{A11}}{\partial k_T^\alpha \partial k_T^\beta}\bigg|_{k_T=0} = \alpha_{em}e_q^2\alpha_s^2\frac{C_F}{N_c^2}8(2\pi)^2\frac{1+z^2}{1-z}\frac{1}{q_T^4}\left[z^2\overline{I}_{A11} + z(1-2z)x_t\frac{\partial \overline{I}_{A11}}{\partial x_C}\right.$$
$$\left. + \ z(1-z)x_t\frac{\partial \overline{I}_{A11}}{\partial x_D} + z^2x_t^2\frac{\partial^2 \overline{I}_{A11}}{\partial x_C^2}\right]_{x_C=0,x_D=0}, \qquad (23)$$

of which the leading contribution in the limit $x_t \sim q_T^2/Q^2 \ll 1$ comes from the first term. However, in the limit $x_t p^+ \ll 1/R_A$, LPM interference becomes important and all the terms are equally important. In this region, non-perturbative effects also become dominant and the medium modification cannot be calculable anymore. In our higher-twist approach, we simply assume the medium modification is still given by the first term in the above equation that do not involve derivatives of the quark-gluon correlation functions. Under this assumption, the hard part from the first diagram in Fig. 4 is then

$$-\frac{1}{4}g^{\alpha\beta}\frac{\overline{H}_{A11}}{\partial k_T^\alpha \partial k_T^\beta}\bigg|_{k_T=0} = \alpha_{em}e_q^2\alpha_s^2\frac{C_F}{N_c^2}8(2\pi)^2\frac{1+z^2}{1-z}\frac{z^2}{q_T^4}\theta(-y_2^-)\theta(y^- - y_1^-)e^{i(x_B+x_t)p^+y^-}$$
$$\times \ \left[1-e^{-ix_tp^+(y^- - y_1^-)}\right]\left[1-e^{-ix_tp^+y_2^-}\right]. \qquad (24)$$

Calculation for the rest of the diagrams and their interferences in Fig. 4 can be similarly carried out. Summing these contributions together, one can obtain the twist-4 contributions from the annihilation-like processes,

$$-\frac{1}{4}g^{\alpha\beta}\frac{\overline{H}_{A}}{\partial k_T^\alpha \partial k_T^\beta}\bigg|_{k_T=0} = \alpha_{em}e_q^2\alpha_s^2\frac{1+z^2}{1-z}\frac{8(2\pi)^2}{N_c^2}\theta(-y_2^-)\theta(y^- - y_1^-)e^{i(x_B+x_t)p^+y^-}$$
$$\times \ \frac{1}{q_T^4}\left[C_Fz^2\left(1-e^{-ix_tp^+(y^- - y_1^-)}\right)\left(1-e^{-ix_tp^+y_2^-}\right)\right.$$
$$+ \ C_Fe^{-ix_tp^+(y^- - y_1^-)}e^{-ix_tp^+y_2^-}$$
$$+ \ \left(C_F - \frac{C_A}{2}\right)z\left(1-e^{-ix_tp^+(y^- - y_1^-)}\right)e^{-ix_tp^+y_2^-}$$
$$+ \ \left(C_F - \frac{C_A}{2}\right)ze^{-ix_tp^+(y^- - y_1^-)}\left(1-e^{-ix_tp^+y_2^-}\right)$$
$$\left. + \ \mathcal{O}(q_T^2/Q^2)\right], \qquad (25)$$

where the color factor $C_A = 3$. The first two terms correspond to the first two diagrams in Fig. 4, respectively. The interferences between these two diagrams are given by the third

and fourth term. However, the diagram containing triple-gluon interaction gives power suppressed contributions q_T^2/Q^2 as compared to the other two diagrams and is therefore neglected. This is quite different from the final state multiple interaction in the nuclear DIS [7] where the dominant contribution due to induced gluon radiation is from the triple-gluon diagram. In contributions from the first two diagrams there are double-hard, soft-hard processes for each diagram. Here the second hard interaction refers to the quark-anti-quark annihilation into DY lepton pair and the initial interaction with the target gluon can be soft or hard, depending on the momentum fraction carried by the initial gluon. The first term has four contributions that include the interferences between the double-hard and soft-hard processes. For the second diagram, however, the soft-hard process is prohibited since the radiated gluon can only be induced by the first hard scattering. In this case, only double-hard process contributes. Notice that one can also obtain the double-hard contributions by considering two successive parton scatterings in a physical gauge as we demonstrate in Appendix C. Using the above equation, we can get the leading twist-four contributions from annihilation-like processes to the DY differential cross section,

$$\begin{aligned}\frac{d\sigma^{DA(R)}_{hA\to\gamma^*}}{dQ^2dx'} &= \sum_q \int dx H_0(x,p,q)\int_0^{\mu^2}\frac{dq_T^2}{q_T^4}\frac{\alpha_s}{2\pi}\int_{x'}^1\frac{d\xi}{\xi}f_{q/h}(\xi)P_{q\to qg}(x'/\xi)\frac{2\pi\alpha_s}{N_c}\\ &\times \left[z^2T_{g\bar q}(x,x_t)+T^{(1)}_{g\bar q}(x,x_t)+\left(1-\frac{C_A}{2C_F}\right)zT^{(2)}_{g\bar q}(x,x_t)\right],\end{aligned} \tag{26}$$

where the nuclear twist-four matrix elements are defined as

$$\begin{aligned}T_{g\bar q}(x,x_t) &= \int\frac{dy^-}{2\pi}dy_1^-dy_2^-e^{i(x+x_t)p^+y^-}\left(1-e^{-ix_tp^+(y^--y_1^-)}\right)\left(1-e^{-ix_tp^+y_2^-}\right)\\ &\times \frac{1}{2}\langle A|F_\alpha^+(y_2^-)\bar\psi_q(0)\gamma^+\psi_q(y^-)F^{+\alpha}(y_1^-)|A\rangle\theta(-y_2^-)\theta(y^--y_1^-),\end{aligned} \tag{27}$$

$$\begin{aligned}T^{(1)}_{g\bar q}(x,x_t) &= \int\frac{dy^-}{2\pi}dy_1^-dy_2^-e^{ixp^+y^-}e^{ix_tp^+(y_1^--y_2^-)}\\ &\times \frac{1}{2}\langle A|F_\alpha^+(y_2^-)\bar\psi_q(0)\gamma^+\psi_q(y^-)F^{+\alpha}(y_1^-)|A\rangle\theta(-y_2^-)\theta(y^--y_1^-),\end{aligned} \tag{28}$$

$$\begin{aligned}T^{(2)}_{g\bar q}(x,x_t) &= \int\frac{dy^-}{2\pi}dy_1^-dy_2^-e^{i(x+x_t)p^+y^-}\left[e^{-ix_tp^+y_2^-}-2e^{-ix_tp^+(y^--y_1^-+y_2^-)}+e^{-ix_tp^+(y^--y_1^-)}\right]\\ &\times \frac{1}{2}\langle A|F_\alpha^+(y_2^-)\bar\psi_q(0)\gamma^+\psi_q(y^-)F^{+\alpha}(y_1^-)|A\rangle\theta(-y_2^-)\theta(y^--y_1^-).\end{aligned} \tag{29}$$

Here $T_{g\bar q}$ and $T^{(1)}_{g\bar q}$ are related to the first and second diagram in Fig. 4, respectively, and $T^{(2)}_{g\bar q}$ arises from the interference between them. Note that the interference between the soft-hard and double hard processes depend on the nuclear size and the momentum fraction x_t from either the target quark or gluon that is needed for the induced gluon radiation. The interference can be neglected when $x_tp^+R_A \gg 1$ for large values of q_T or short formation length for the gluon radiation relative to the nuclear size. In the small q_T region or large formation time, however, the interference effect becomes important due to what is referred to as LPM effect [40]. The destructive interference is dictated by the gluon formation time, $\tau_f \equiv 1/x_tp^+$, which, in the collinear limit, could become much larger than the relative

distance between the two scattering centers. Therefore the LPM effect will effectively cut off the transverse momentum of the virtual photon at $q_T^2 \sim Q^2/R_A$ [7] in the leading calculation of the DY lepton pair production. This will lead to an anomalous nuclear dependence of the DY cross section in $h + A$ collisions.

We also need to consider the interferences between single and triple scattering. Our calculations show that all the contributions from these processes are power suppressed because the leading term, i.e., the last term in Eq. (22), vanishes. However, when combining all the contributions from both the double scattering and single-triple interferences, the first term in the collinear expansion in Eq. (14) gives the eikonal contributions to the single scattering. Such contributions do not correspond to any physical scattering since they can be gauged away, but ensures the gauge invariance of the leading twist results. We list the full results of the single-triple interferences in the appendix.

Similarly to the leading twist case, one also needs to consider the virtual contribution which corresponds to the quark self-energy correction. The results of virtual correction can be obtained by the requirement of unitarity.

$$\begin{aligned}\frac{d\sigma^{DA(V)}_{hA\to\gamma^*}}{dQ^2dx'} &= -\sum_q \int dx H_0(x,p,q) \int_0^{\mu^2} \frac{dq_T^2}{q_T^4}\frac{\alpha_s}{2\pi}\int_0^1 dz f_{q/h}(x')P_{q\to qg}(z)\frac{2\pi\alpha_s}{N_c} \\ &\times \left[z^2 T_{g\bar q}(x,x_t) + T^{(1)}_{g\bar q}(x,x_t) + \left(1-\frac{C_A}{2C_F}\right) z T^{(2)}_{g\bar q}(x,x_t)\right]. \end{aligned} \tag{30}$$

Including both radiative and virtual contributions, the final result for the annihilation-like process is given by

$$\frac{d\sigma^{DA}_{hA\to\gamma^*}}{dQ^2dx'} = \sum_q \int dx f_{\bar q/A}(x) \int_0^{\mu^2}\frac{dq_T^2}{q_T^2}\frac{\alpha_s}{2\pi}\int_{x'}^1 \frac{d\xi}{\xi} f_{q/h}(\xi)\Delta\gamma_{q\to qg}(x'/\xi, q_T^2) H_0(x,p,q)\,. \tag{31}$$

Here, the modified quark splitting function is

$$\Delta\gamma_{q\to qg}(z,q_T^2) = \left[\frac{1+z^2}{(1-z)_+} T^A_{g\bar q} + \delta(1-z)\Delta T^A_{g\bar q}\right]\frac{C_F 2\pi\alpha_s}{q_T^2 N_c f_{\bar q/A}(x)} \tag{32}$$

with

$$T^A_{g\bar q} = z^2 T_{g\bar q}(x,x_t) + T^{(1)}_{g\bar q}(x,x_t) + \left(1-\frac{C_A}{2C_F}\right) z T^{(2)}_{g\bar q}(x,x_t) \tag{33}$$

and

$$\Delta T^A_{g\bar q} \equiv \int_0^1 dz \frac{1}{1-z}\left[2T^A_{g\bar q}|_{z=1} - (1+z^2)T^A_{g\bar q}\right]. \tag{34}$$

Notice that the infrared divergence is canceled between the real and virtual corrections in the same way as in the single scattering.

The other twist-four processes that contribute to the modified beam quark distribution function are the Compton-like processes as shown in Fig. 5. The full results of these processes can be found in the appendix. Similarly to the calculation of annihilation-like processes, one can get the leading twist-4 contributions,

$$-\frac{1}{4} g^{\alpha\beta}\frac{\overline{H}_C}{\partial k_T^\alpha \partial k_T^\beta}\bigg|_{k_T=0} = \alpha_{em} e_q^2 \alpha_s^2 (2z^2 - 2z + 1)\frac{8(2\pi)^2}{N_c(N_c^2-1)} e^{i(x_B+x_t)p^+y^-}\theta(-y_2^-)\theta(y^- - y_1^-)$$

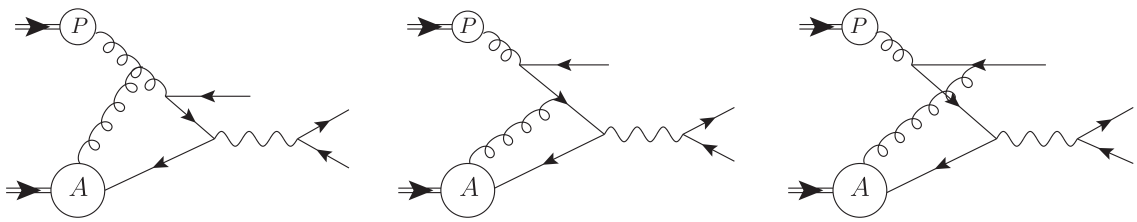

FIG. 5: Next-to-leading order Drell-Yan compton process at twist-four.

$$\times \ \frac{1}{q_T^4}\left[C_A z^2\left(1-e^{-ix_tp^+(y^--y_1^-)}\right)\left(1-e^{-ix_tp^+y_2^-}\right)\right.$$
$$+ \ C_F e^{-ix_tp^+(y^--y_1^-)}e^{-ix_tp^+y_2^-}+\frac{C_A}{2}z\left(1-e^{-ix_tp^+(y^--y_1^-)}\right)e^{-ix_tp^+y_2^-}$$
$$\left.+ \ \frac{C_A}{2}ze^{-ix_tp^+(y^--y_1^-)}\left(1-e^{-ix_tp^+y_2^-}\right)+\mathcal{O}(q_T^2/Q^2)\right]. \qquad (35)$$

which are analogous to the results from the annihilation-like processes. The first two terms correspond to the first two diagrams in Fig. 5, respectively. The third and fourth terms are the interference contributions between the two diagrams. The contribution from the last diagram in Fig. 5 is neglected as its contribution is power suppressed. Again, one can obtain the double-hard contributions by considering two successive single scatterings as shown in Appendix C. Using the above results, for Compton-like process, Eq. (15) finally reads

$$\frac{d\sigma^{DC}_{hA\to l^+l^-}}{dQ^2dx'} = \sum_q\int dx f_{\bar q/A}(x)\int_0^{\mu^2}\frac{dq_T^2}{q_T^2}\frac{\alpha_s}{2\pi}\int_{x'}^1\frac{d\xi}{\xi}f_{g/h}(\xi)\Delta\gamma_{g\to q\bar q}(x'/\xi,q_T^2)H_0(x,p,q), \qquad (36)$$

where the modified gluon splitting function is defined as

$$\Delta\gamma_{g\to q\bar q}(z,q_T^2)=\left[(1-z)^2+z^2\right]T^C_{g\bar q}\frac{2\pi\alpha_s C_A}{q_T^2(N_c^2-1)f_{\bar q/A}(x)}, \qquad (37)$$

with the twist-four matrix element

$$T^C_{g\bar q}=z^2T_{g\bar q}(x,x_t)+\frac{C_F}{C_A}T^{(1)}_{g\bar q}(x,x_t)+\frac{1}{2}zT^{(2)}_{g\bar q}(x,x_t). \qquad (38)$$

Diagrams in Fig. 5 contributing to each term in the above equation are similar to the annihilation-like processes. Here, the twist-four matrix elements are the same as in the annihilation-like processes as defined in Eq. (27)-(29). In Compton-like processes, there is no virtual correction at $\mathcal{O}(\alpha_s)$, and the gluon splitting function is infrared finite.

IV. MODIFIED QUARK DISTRIBUTION FUNCTION

Summing up all the leading logarithmic contributions from single [Eq. (8)] and double scattering [Eqs. (31) and (36)], we can define the medium-modified effective beam quark distribution function as

$$\tilde f_{q/h}(x',\mu^2,A) = f_{q/h}(x',\mu^2)+\frac{\alpha_s}{2\pi}\int_0^{\mu^2}\frac{dq_T^2}{q_T^2}\int_{x'}^1\frac{d\xi}{\xi}\left[f_{q/h}(\xi)\Delta\gamma_{q\to qg}(x'/\xi,q_T^2)\right.$$
$$\left.+ \ f_{g/h}(\xi)\Delta\gamma_{g\to q\bar q}(x'/\xi,q_T^2)\right], \qquad (39)$$

where $f_{q/h}(x', \mu^2)$ is the renormalized twist-two beam quark distribution given in Eq. (8). The A-dependence of the medium-modified beam quark distribution function is implicit through the medium-modified splitting functions in the second term on the right-hand side. Assuming that multiple gluon bremsstrahlung induced by additional scattering in the nuclear medium can be resummed in the same way as in the vacuum, one can obtain the medium-modified DGLAP evolution equation for the beam quark distribution function

$$\frac{\partial \tilde{f}_{q/h}(x', \mu^2, A)}{\partial ln\mu^2} = \frac{\alpha_s}{2\pi}\int_{x'}^{1}\frac{d\xi}{\xi}\left[\tilde{f}_{q/h}(\xi,\mu^2)\tilde{\gamma}_{q\to qg}(x'/\xi,\mu^2) + \tilde{f}_{g/h}(\xi,\mu^2)\tilde{\gamma}_{g\to q\bar{q}}(x'/\xi,\mu^2)\right], \quad (40)$$

where the modified splitting functions,

$$\tilde{\gamma}_{a\to bc}(z,\mu^2) = \gamma_{a\to bc}(z) + \Delta\gamma_{a\to bc}(z,\mu^2), \quad (41)$$

are the sum of contributions from both the vacuum and the nuclear medium-induced bremsstrahlung. Notice that Eq. (40) is formally the same as the DGLAP evolution equation in vacuum, Eq. (11), but its splitting functions have extra terms $\Delta\gamma$ which are caused by medium-induced gluon radiation. Such medium-induced terms will soften the beam quark distribution function as a consequences of radiative energy loss by the leading beam parton.

As we mentioned before, the medium-modified splitting functions $\Delta\gamma$ depend on the twist-four matrix elements $T^A_{g\bar{q}}$. In order to get a numerical estimate of the effect of initial parton energy loss, we need to know $T^A_{g\bar{q}}$ which is not calculable. Neglecting correlation between the quark and gluon distribution, one can assume the factorization of the twist-four matrix elements [15] in terms of quark and gluon distributions [4] from two independent nucleons inside the nucleus, the later in turn can be related to quark transport parameter $\hat{q}$ in nuclear medium. Under these assumptions, the twist-four matrix elements can be expressed as

$$\begin{aligned} T_{g\bar{q}}(x,x_t) &= 2\pi\int_{-\infty}^{\infty}dy^-\int_0^{\infty}d^2b\int_{-\infty}^{y^-}dy_1^-\rho_A(y_1^-,\vec{b})\rho_A(y^-,\vec{b}) \\ &\times\ \sin^2(x_t p^+ y_1^-/2) f^A_{\bar{q}/N}(x,\vec{b})\left[x f^A_{g/N}(x,\vec{b})|_{x\approx 0} + x_t f^A_{g/N}(x_t,\vec{b})\right], \end{aligned} \quad (42)$$

where, $f^A_{a/N}(x,\vec{b})$ is the parton distribution function per nucleon inside the nucleus. As illustrated in Fig. 6, $\vec{b}$ is the impact parameter of $h + A$ collisions, y_1^- is the longitudinal position of the target nucleon where the soft gluon comes from and y^- is the longitudinal position of the target nucleon where the final quark-antiquark annihilation into DY lepton pair takes place. One has to integrate over the impact parameter $\vec{b}$. The nucleon density distribution $\rho_A(y^-,\vec{b})$ is normalized as

$$A = \int_{-\infty}^{\infty}dy^-\int_0^{\infty}d^2b\,\rho_A(y^-,\vec{b}). \quad (43)$$

So far we have focused on the nuclear modification of beam quark distribution function in DY processes in $h + A$ collisions due to multiple parton scattering and medium-induced parton energy loss. Multiple parton interaction and their coherence can also lead to nuclear modification of the target parton distributions. Gluon fusion in the evolution of the target parton distribution function can also lead to parton saturation [52]. Some of these effects are higher-twist as we have discussed so far and some are leading twist which are determined by the wave function of the nucleus and initial parton distribution functions. In this paper,

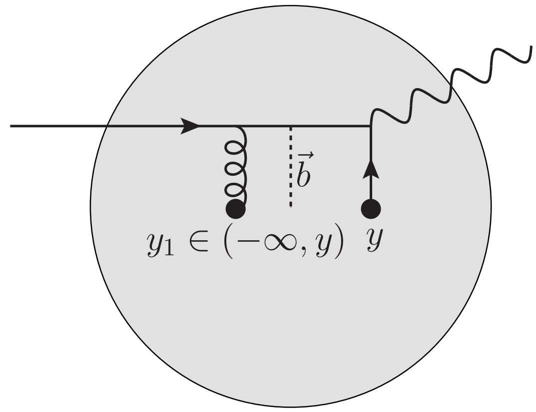

FIG. 6: Illustration of PA scattering.

we will adopt a phenomenological approach for the nuclear modification of the target parton distributions and use the current parameterization of the nuclear parton distribution functions (nPDF) from global fit to the existing experimental data. In this case, the effective target parton distribution function per nucleon at impact parameter $\vec{b}$ is defined as

$$f^A_{a/N}(x,\vec{b}) \equiv \frac{1}{A} f_{a/A}(x,\vec{b}) \equiv R^a_A(x,\vec{b}) f_{a/N}(x), \tag{44}$$

where $f_{a/N}(x)$ is the nucleon parton distribution function in vacuum and $R^a_A(x,\vec{b})$ is the nuclear modification factor for parton distribution functions inside a nucleus at impact parameter $\vec{b}$. The impact parameter averaged parton distribution function in a nucleus is defined as

$$f_{a/A}(x) \equiv f_{a/N}(x) \int d^2b t_A(\vec{b}) R^a_A(x,\vec{b}), \tag{45}$$

where $t_A(\vec{b}) = \int dy^- \rho_A(y^-,\vec{b})$ is the nuclear thickness function. Note that the nuclear modification factor $R^a_A(x,\vec{b})$ should contain the information about the isospin of the nucleus.

We further define the generalized jet transport parameter as

$$\begin{aligned}\hat{q}(x_t,y^-,\vec{b}) \;&\equiv\; \frac{4\pi^2\alpha_s C_R}{N_c^2-1}\rho_A(y^-,\vec{b})\frac{1}{2}\left[x f^A_{g/N}(x,\vec{b})|_{x\approx 0} + x_t f^A_{g/N}(x_t,\vec{b})\right] \\ &\approx\; \hat{q}_0 \frac{\rho_A(y^-,\vec{b})}{\rho_A(0,\vec{0}_\perp)},\end{aligned} \tag{46}$$

assuming the limit $x_t \ll 1$, where $\hat{q}_0$ is the quark transport parameter in the center of the nucleus. With the above definition of quark transport parameter and nuclear quark distribution function, the twist-four matrix elements can be expressed as,

$$\begin{aligned}T_{g\bar{q}}(x,x_t) \;&\approx\; \frac{6\hat{q}_0 f_{\bar{q}/N}(x)}{\pi\alpha_s\rho_A(0,\vec{0}_\perp)} \int d^2b \int_{-\infty}^{\infty} dy^- \int_{-\infty}^{y^-} dy_1^- \rho_A(y_1^-,\vec{b})\rho_A(y^-,\vec{b}) \\ &\times\; \sin^2(x_t p^+ y_1^-/2) R^{\bar{q}}_A(x,\vec{b}).\end{aligned} \tag{47}$$

In our numerical evaluation, we will use the Woods-Saxon distribution for the nucleon distribution

$$\rho_A(y,\vec{b}) = \frac{\rho_0}{1+\exp(\frac{r-R_A}{a})}, \tag{48}$$

where $r = \sqrt{b^2 + y^2}$, $R_A \approx 1.12A^{1/3}$ fm is the radius of the nucleus, $a \approx 0.537$ the width of the nuclear skin and the constant ρ_0 is fixed by normalization in Eq. (43).

Similarly, the other two matrix elements in Eqs. (28) and (29) can be approximated as

$$T^{(1)}_{g\bar{q}}(x_B, x_t) \approx \frac{3\hat{q}_0 f_{\bar{q}/N}(x)}{2\pi\alpha_s\rho_A(0, \vec{0}_\perp)} \int d^2b \int_{-\infty}^{\infty} dy^- \int_{-\infty}^{y^-} dy_1^- \rho_A(y_1^-, \vec{b})\rho_A(y^-, \vec{b}) R_A^{\bar{q}}(x, \vec{b}), \quad (49)$$

$$T^{(2)}_{g\bar{q}}(x_B, x_t) \approx \frac{-6\hat{q}_0 f_{\bar{q}/N}(x)}{\pi\alpha_s\rho_A(0, \vec{0}_\perp)} \int d^2b \int_{-\infty}^{\infty} dy^- \int_{-\infty}^{y^-} dy_1^- \rho_A(y_1^-, \vec{b})\rho_A(y^-, \vec{b}) \times \sin^2(x_t p^+ y_1^-/2) R_A^{\bar{q}}(x, \vec{b}). \quad (50)$$

Because of the LPM interference effect, the formation time for the induced parton radiation cannot be larger than the nuclear size. This will restrict the transverse momentum q_T to a limited region $q_T^2 \sim Q^2/A^{1/3}$. Below this limit, the contributions will be suppressed because of the destructive LPM interference. Such LPM effect in contributions that contain $T_{g\bar{q}}$ and $T^{(2)}_{g\bar{q}}$ give rise to an addition factor of $A^{1/3}$ after integration over the transverse momentum. This nuclear enhancement leads to the quadratic nuclear size dependence of the parton energy loss. Relative to these two contributions and in the large nucleus limit, we can neglect contributions proportional to $T^{(1)}_{g\bar{q}}$ which does not contain LPM effect [8].

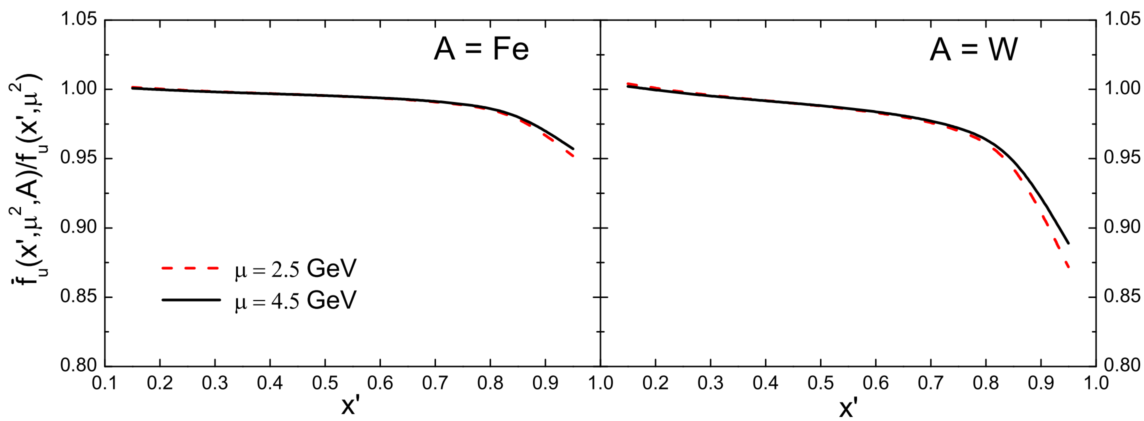

FIG. 7: Nuclear modification of the effective beam u-quark distribution functions $\tilde{f}_u(x', \mu^2, A)/f_u(x', \mu^2)$ versus x' in DY processes in $p + A$ collisions at $E_{lab} = 800$ GeV and scale $\mu = 4.5$ (solid) and 2.5 GeV (dashed). The quark transport parameter is set at $\hat{q}_0 = 0.024$ GeV^2/fm[15].

Shown in Fig. 7 are the effective nuclear modification factors of the beam u-quark distributions in $p + W$ and $p + Fe$ DY processes at $E_{\rm lab} = 800$ GeV. In this numerical calculation and in the rest of this paper, we will only consider the effective nuclear modified beam parton distributions due to double scattering as given in Eq. (39). The normal twist-2 quark distributions in nucleon are given by the CTEQ6L [53] parameterization, the nuclear modification of parton distribution functions inside a nuclear target will be given by the EPS08 [43] parameterization without impact-parameter dependence. As shown in the figure, the nuclear modification of the beam quark distribution function is negligible in small x' region. The modification becomes significant in the large x' region for small factorization scale μ and large target nuclei. We also observe some small scale dependence of the nuclear modification.

Experimentally, the Drell-Yan differential cross section can be measured for different targets in hadron-nucleus collisions. The cross section ratios are analyzed for the study of nuclear effects,

$$\frac{B\sigma^A}{A\sigma^B} = \frac{Bd\sigma_{pA\to l^+l^-}/dQ^2dx'}{Ad\sigma_{pB\to l^+l^-}/dQ^2dx'}. \tag{51}$$

In general, one would like to use the experimental data in $p+p$ collisions as the reference in the denominator to study the nuclear effects in $p+A$ collisions with a large nucleus target. One, however, often uses $p+B$ with a light nucleus target B as an approximate of the $p+p$ reference data (modulo isospin corrections) as in the Fermilab E866 [32] experiment. Under this approximation, the measured nuclear modification can be compared to

$$\frac{B\sigma^A}{A\sigma^B} = \frac{\sum_q \int dx f_{\bar{q}/A}(x,\mu^2)\tilde{f}_{q/p}(x',\mu^2,A)H_0(x,p,q)}{A\sum_q \int dx f_{\bar{q}/N}(x,\mu^2)f_{q/p}(x',\mu^2)H_0(x,p,q)}, \tag{52}$$

where $\tilde{f}_{q/p}(x',\mu^2,A)$ is the modified beam quark distribution function defined in Eq. (39), and $f_{\bar{q}/N}(x,\mu^2)$ is the normal twist-2 anti-quark distribution in nucleon (with the isospin of the nucleus B) which will be given by the CTEQ6L [53] parameterization in our study here. As for the nuclear modification of parton distribution functions inside a nuclear target, we will use the EPS08 [43] parameterization without impact-parameter dependence.

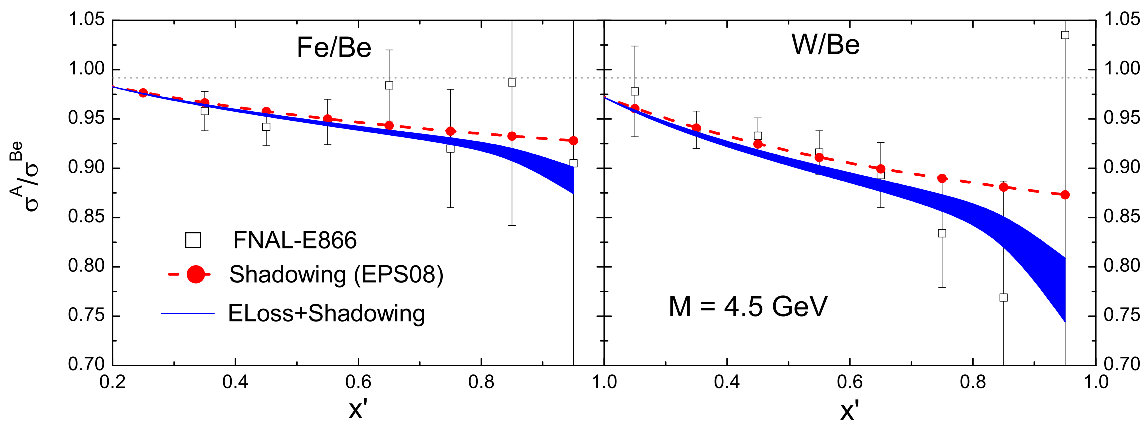

FIG. 8: Ratios of the DY cross section per nucleon in $p+A$ collisions versus x' for Fe/Be and W/Be at $E_{lab} = 800$ GeV and invariant dilepton mass $M = 4.5$ GeV. The curves are theoretical results with (solid) and without (dashed) initial beam parton energy loss. The shaded bands correspond to $\hat{q}_0 = 0.024 \pm 0.008$ GeV^2/fm [15]. The experimental data are from the Fermilab experiment E866 [32].

Shown in Fig. 8 are the calculated DY cross section ratios as a function of x' for different nuclei (Be, Fe and W) with (solid) and without (dashed) the effect of initial beam parton energy loss via multiple interaction, as compared to the Fermilab E866 experimental data [32]. In our numerical evaluation of the effect of initial beam parton energy loss, the quark transport parameter $\hat{q}_0$ at the center of a large nucleus is the only free parameter and is fixed to $\hat{q}_0 = 0.024 \pm 0.008\,\text{GeV}^2/\text{fm}$ from the phenomenological study of parton energy loss and modified fragmentation function in nuclear DIS by the HERMES experiment [15]. As shown

in the comparison between our calculation and the experimental data in the kinematic region of the E866 experiment, the dominant nuclear modification of the DY cross section is from nuclear shadowing of parton distribution functions inside large nuclei as given by the EPS08 [43] parameterization. For fixed invariant mass M, the fractional momentum $x = M^2/x's$ carried by the target partons becomes smaller for large beam quark fractional momentum x', therefore strong nuclear shadowing of the quark distribution inside the target nucleus. The effect of medium-modified beam quark distribution caused by beam quark energy loss leads to further suppression of the DY cross section for large nuclei. However, with the quark transport parameter predetermined from the nuclear DIS experiment [15], the suppression due to initial beam quark energy loss is quantitatively small. This is consistent with other estimates of parton energy loss in DY process [33–35]. The additional suppression only becomes considerable in large x' region in a large nucleus where one also see large nuclear modification of the effective beam quark distribution function as shown in Fig. 7. Since the parameterization of nPDF [43] from global fitting included DY data, one should include the effect of beam parton energy loss in large x' or small x region.

Without initial beam parton energy loss, the nuclear modification of the DY cross section as a function of the target parton momentum fraction x should more or less reflect that of the parton shadowing, which is shown in the left panel of Fig. 9. The slight x-scaling violation for different invariant DY dilepton mass M is caused mainly by the scale violation of the parton shadowing effect as given by the EPS08 [43] parameterization. Parton shadowing becomes smaller for larger invariant mass due to the QCD evolution of the nuclear parton distributions which leads to less suppression of the DY cross section. When one takes into account of the beam parton energy loss, there is increased suppression of DY cross section at large x' or small x for fixed invariant mass M as shown in the right panel of Fig. 9. For fixed values of x, an increase of invariant mass M leads to an increase in x'. This should lead in turn an increased suppression due to beam parton energy loss according to Figs. 8. Such increased suppression due to larger values of x' will counter the effect of scale violation of the shadowing (see the left panel). The final outcome is an approximate x-scaling of the suppression factor in small x region for different values of the DY dilepton mass.

Nuclear shadowing of parton distributions in the target nucleus is significant only at small momentum fraction x. For fixed invariant mass of DY lepton pairs and moderately large beam parton momentum fraction x' or large target parton momentum fraction x, the effect of shadowing should be small. On the other hand the fractional parton energy loss will become larger for smaller beam parton energy $x'E_{lab}$ [15]. Therefore, at fixed DY dilepton mass M and moderately large beam parton momentum fraction x', the effect of the parton energy loss on DY cross section in $p+A$ collisions will become more dominant for lower beam energy E_{lab}. This will enable one to disentangle the effect of initial-state energy loss effect from the nuclear shadowing. Shown in Fig. 10 are the predictions for the DY cross section ratios at $E_{lab} = 120$ GeV in the Fermilab's E906 experiment [54, 55] with invariant dilepton mass $M = 4.5$ GeV. At this lower beam proton energy, the target parton momentum fraction x is large for moderately large beam parton fractional momentum x'. The effect of parton shadowing is indeed small as shown by the dashed line in Fig. 10. On the other hand, the energy loss effect induced by multiple scattering is significant and the dominant cause for the DY suppression shown by the shaded bands in Fig. 10. Therefore, the E906 experiment can provide an unambiguous measurement of the effect of initial state energy loss in DY cross section. This is consistent with another recent predictions of the energy loss effects at the E906 experiment [37].

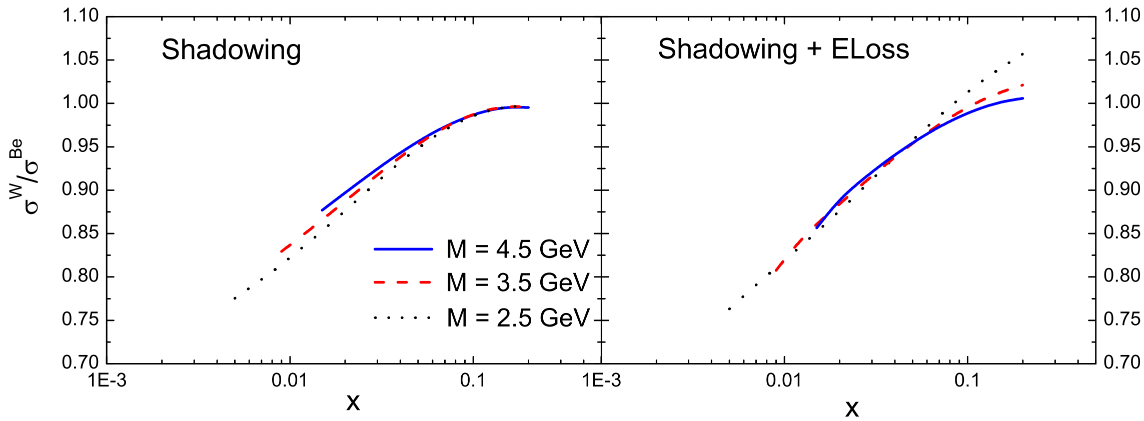

FIG. 9: Ratios of the DY cross section per nucleon in p+W and p+Be collisions versus x at E_{lab} = 800 GeV for invariant dilepton mass M = 4.5 (solid), 3.5 (dashed) and 2.5 (doted) GeV with only parton shadowing (left panel) and shadowing and initial beam parton energy loss (right panel). The quark transport parameter is set at $\hat{q}_0 = 0.024$ GeV$^2/fm$ [15].

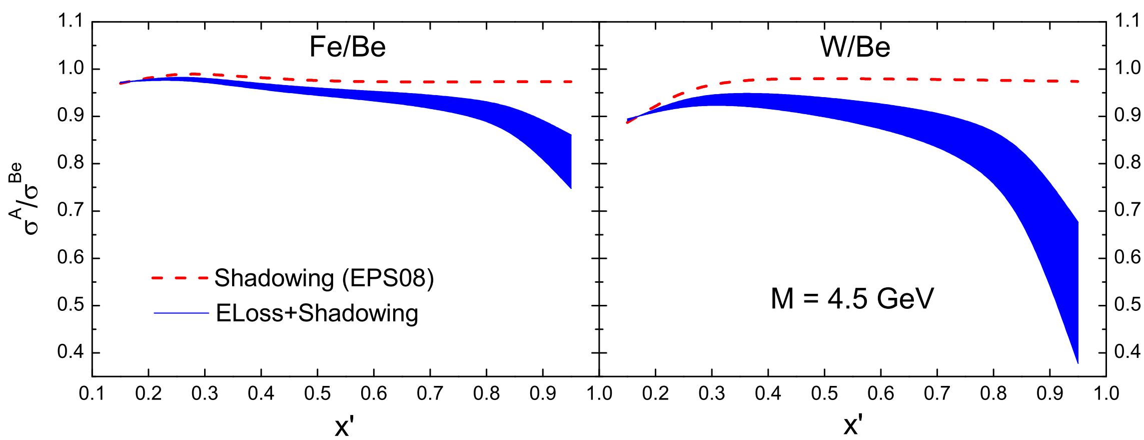

FIG. 10: Predictions for the DY cross section ratios per nucleon in $p + A$ collisions versus x' for Fe/Be and W/Be at (E_{lab} = 120 GeV) with invariant dilepton mass M = 4.5 GeV. The curves are theoretical results with (solid) and without (dashed) initial beam parton energy loss. The shaded bands correspond to $\hat{q}_0 = 0.024 \pm 0.008$ GeV^2/fm [15].

V. SUMMARY

In this paper, we have calculated the differential cross section of the Drell-Yan dilepton production in hadron-nucleus collisions in the lowest order of pQCD, including the effect of initial multiple parton scattering and induced gluon radiation within the framework of generalized collinear factorization. In nuclear medium, multiple parton scattering leads to energy loss of the beam parton which has a quadratic nuclear size dependence because of the LPM interference effect. Within the leading logarithmic approximation, we express the effect of parton energy loss in terms of an effective modified beam quark distribution function. The modification depends on the twist-four matrix elements which can be related to the normal

twist-2 parton distributions and jet transport parameter $\hat{q}$. Using the values of $\hat{q}$ determined from nuclear DIS data by the HERMES experiment [15], we found that the effect of initial beam parton energy loss is quite small for large invariant mass of DY lepton pairs in $p + A$ collision at high-energies, except in the large x' region and for heavy nuclear targets. The Fermilab E866 experimental data are consistent with the effect of the nuclear shadowing of target parton distributions as given by the EPS08 parametrization. However, the effect of beam parton energy loss becomes significant for lower beam proton energy $E_{lab} = 120$ GeV at the Fermilab E906 experiment, especially at large x' and with heavy nuclear targets. For parameterization with improved accuracy of nuclear parton distribution functions through consistent global fitting of experiment data, one should also include the effect of initial beam parton energy loss in the DY process.

Acknowledgments

This work is supported by the NSFC of China under Projects Nos. 10825523, 10875025 and MOST of China under project No. 2008CB317106, and by MOE and SAFEA of China under project No. PITDU-B08033, and by the Director, Office of Energy Research, Office of High Energy and Nuclear Physics, Divisions of Nuclear Physics, of the U.S. Department of Energy under Contract No. DE-AC02-05CH11231. The research of Y.G. was supported by the Natural Sciences and Engineering Research Council of Canada.

Appendix

In this appendix we list the complete results for annihilation-like and Compton-like processes, we also provide an cross-check of the double-hard part through partonic quark-gluon and gluon-gluon scattering.

Appendix A: complete results in annihilation-like process

There are total 9 diagrams for central-cut, and 7 diagrams for left- and right-cut each. The central-cut diagrams are shown in Fig. 4 and their contributions are:

$$\overline{H}_{A11} = \alpha_s^2 \alpha_{em} e_q^2 C_F \frac{1+z^2}{1-z} \frac{1}{(\vec{q}_T - z\vec{k}_T)^2} \frac{8(2\pi)^2}{N_c^2} \overline{I}_{A11}, \tag{A1}$$

$$\begin{aligned} \overline{I}_{A11} &= e^{i(x_B+x_t+x_C-x_D)p^+y^-} e^{ix_Dp^+(y_1^- - y_2^-)} \theta(-y_2^-)\theta(y^- - y_1^-) \\ &\times \left[1 - e^{-i(x_t+x_C-x_D)p^+(y^- - y_1^-)}\right] \left[(1 - e^{-i(x_t+x_C-x_D)p^+y_2^-}\right] \end{aligned} \tag{A2}$$

$$\overline{H}_{A22} = \alpha_s^2 \alpha_{em} e_q^2 C_F \frac{1+z^2}{1-z} \frac{1}{(\vec{q}_T - \vec{k}_T)^2} \frac{8(2\pi)^2}{N_c^2} \overline{I}_{A22}, \tag{A3}$$

$$\overline{I}_{A22} = e^{ix_Bp^+y^-} e^{i(x_t+x_C)p^+y_1^-} e^{-i(x_t+x_C)p^+y_2^-} \theta(-y_2^-)\theta(y^- - y_1^-) \tag{A4}$$

$$\overline{H}_{A33} = \alpha_s^2 \alpha_{em} e_q^2 C_A \frac{1+z^2}{1-z} \frac{1}{q_T^2} \frac{8(2\pi)^2}{N_c^2} \overline{I}_{A33}, \tag{A5}$$

$$\overline{I}_{A33} = e^{ix_Bp^+y^-} e^{i(x_t+x_C)p^+y_1^-} e^{-i(x_t+x_C)p^+y_2^-} \theta(-y_2^-)\theta(y^- - y_1^-);$$

$$\overline{H}_{A12} = \alpha_s^2 \alpha_{em} e_q^2 \left(C_F - \frac{C_A}{2}\right) \frac{1+z^2}{1-z} \frac{[q_T^2 - (1+z)\vec{k}_T \cdot \vec{q}_T + zk_T^2]}{(\vec{q}_T - \vec{k}_T)^2 (\vec{q}_T - z\vec{k}_T)^2} \frac{8(2\pi)^2}{N_c^2} \overline{I}_{A12}, \tag{A6}$$

$$
\begin{aligned}
\overline{I}_{A12} &= e^{i(x_B+x_t+x_C-x_D)p^+y^-} e^{ix_Dp^+(y_1^- - y_2^-)}\theta(-y_2^-)\theta(y^- - y_1^-) \\
&\times \left[1 - e^{-i(x_t+x_C-x_D)p^+(y^- - y_1^-)}\right] e^{-i(x_t+x_C-x_D)p^+y_2^-} \qquad \text{(A7)}
\end{aligned}
$$

$$
\overline{H}_{A13} = \alpha_s^2\alpha_{em}e_q^2\frac{C_A}{2}\frac{1+z^2}{1-z}\frac{q_T^2 - z\vec{k}_T\cdot\vec{q}_T}{q_T^2(\vec{q}_T - z\vec{k}_T)^2}\frac{8(2\pi)^2}{N_c^2}\overline{I}_{A13}, \qquad \text{(A8)}
$$

$$
\begin{aligned}
\overline{I}_{A13} &= e^{i(x_B+x_t+x_C-x_D)p^+y^-} e^{ix_Dp^+(y_1^- - y_2^-)}\theta(-y_2^-)\theta(y^- - y_1^-) \\
&\times \left[1 - e^{-i(x_t+x_C-x_D)p^+(y^- - y_1^-)}\right] e^{-i(x_t+x_C-x_D)p^+y_2^-} \qquad \text{(A9)}
\end{aligned}
$$

$$
\overline{H}_{A21} = \alpha_s^2\alpha_{em}e_q^2\left(C_F - \frac{C_A}{2}\right)\frac{1+z^2}{1-z}\frac{q_T^2 - (1+z)\vec{k}_T\cdot\vec{q}_T + zk_T^2}{(\vec{q}_T - \vec{k}_T)^2(\vec{q}_T - z\vec{k}_T)^2}\frac{8(2\pi)^2}{N_c^2}\overline{I}_{A21}, \qquad \text{(A10)}
$$

$$
\begin{aligned}
\overline{I}_{A21} &= e^{i(x_B+x_t+x_C-x_D)p^+y^-} e^{ix_Dp^+(y_1^- - y_2^-)}\theta(-y_2^-)\theta(y^- - y_1^-) \\
&\times e^{-i(x_t+x_C-x_D)p^+(y^- - y_1^-)}\left[(1 - e^{-i(x_t+x_C-x_D)p^+y_2^-}\right] \qquad \text{(A11)}
\end{aligned}
$$

$$
\overline{H}_{A23} = \alpha_s^2\alpha_{em}e_q^2\frac{C_A}{2}\frac{1+z^2}{1-z}\frac{q_T^2 - \vec{k}_T\cdot\vec{q}_T}{q_T^2(\vec{q}_T - \vec{k}_T)^2}\frac{8(2\pi)^2}{N_c^2}\overline{I}_{A23}, \qquad \text{(A12)}
$$

$$
\overline{I}_{A23} = -e^{ix_Bp^+y^-} e^{i(x_t+x_C)p^+y_1^-} e^{-i(x_t+x_C)p^+y_2^-}\theta(-y_2^-)\theta(y^- - y_1^-) \qquad \text{(A13)}
$$

$$
\overline{H}_{A31} = \alpha_s^2\alpha_{em}e_q^2\frac{C_A}{2}\frac{1+z^2}{1-z}\frac{q_T^2 - z\vec{k}_T\cdot\vec{q}_T}{q_T^2(\vec{q}_T - z\vec{k}_T)^2}\frac{8(2\pi)^2}{N_c^2}\overline{I}_{A31}, \qquad \text{(A14)}
$$

$$
\begin{aligned}
\overline{I}_{A31} &= e^{i(x_B+x_t+x_C-x_D)p^+y^-} e^{ix_Dp^+(y_1^- - y_2^-)}\theta(-y_2^-)\theta(y^- - y_1^-) \\
&\times e^{-i(x_t+x_C-x_D)p^+(y^- - y_1^-)}\left[(1 - e^{-i(x_t+x_C-x_D)p^+y_2^-}\right] \qquad \text{(A15)}
\end{aligned}
$$

$$
\overline{H}_{A32} = \alpha_s^2\alpha_{em}e_q^2\frac{C_A}{2}\frac{1+z^2}{1-z}\frac{q_T^2 - \vec{k}_T\cdot\vec{q}_T}{q_T^2(\vec{q}_T - \vec{k}_T)^2}\frac{8(2\pi)^2}{N_c^2}\overline{I}_{A32}, \qquad \text{(A16)}
$$

$$
\overline{I}_{A32} = -e^{ix_Bp^+y^-} e^{i(x_t+x_C)p^+y_1^-} e^{-i(x_t+x_C)p^+y_2^-}\theta(-y_2^-)\theta(y^- - y_1^-). \qquad \text{(A17)}
$$

All the left-cut diagrams in annihilation-like process are shown in Fig. 11 and their contributions are:

$$
\overline{H}_{AL1} = \alpha_s^2\alpha_{em}e_q^2C_F\frac{1+z^2}{1-z}\frac{1}{q_T^2}\frac{8(2\pi)^2}{N_c^2}\overline{I}_{L1}, \qquad \text{(A18)}
$$

$$
\overline{I}_{AL1} = -e^{i(x_B+x_t)p^+y^-} e^{-ix_Dp^+(y_1^- - y_2^-)}\left[1 - e^{-ix_tp^+y_2^-}\right]\theta(-y_2^-)\theta(y_2^- - y_1^-); \qquad \text{(A19)}
$$

$$
\overline{H}_{AL2} = \alpha_s^2\alpha_{em}e_q^2\left(C_F - \frac{C_A}{2}\right)\frac{1+z^2}{1-z}\frac{q_T^2 - (1-z)\vec{k}_T\cdot\vec{q}_T}{q_T^2[\vec{q}_T - (1-z)\vec{k}_T]^2}\frac{8(2\pi)^2}{N_c^2}\overline{I}_{L2}, \qquad \text{(A20)}
$$

$$
\begin{aligned}
\overline{I}_{AL2} &= e^{i(x_B+x_t)p^+y^-} e^{-ix_Dp^+(y_1^- - y_2^-)}\theta(-y_2^-)\theta(y_2^- - y_1^-); \\
&\times e^{-ix_tp^+y_2^-}\left[e^{i(x_E-x_t+x_D)p^+(y_1^- - y_2^-)} - 1\right]; \qquad \text{(A21)}
\end{aligned}
$$

$$
\overline{H}_{AL3} = \alpha_s^2\alpha_{em}e_q^2\frac{C_A}{2}\frac{1+z^2}{1-z}\frac{q_T^2 + z\vec{k}_T\cdot\vec{q}_T}{q_T^2(\vec{q}_T + z\vec{k}_T)^2}\frac{8(2\pi)^2}{N_c^2}\overline{I}_{L3}, \qquad \text{(A22)}
$$

$$
\begin{aligned}
\overline{I}_{AL3} &= e^{i(x_B+x_t)p^+y^-} e^{-ix_Dp^+(y_1^- - y_2^-)}\theta(-y_2^-)\theta(y_2^- - y_1^-) \\
&\times e^{-ix_tp^+y_2^-}\left[e^{i(-x_F-x_t+x_D)p^+(y_1^- - y_2^-)} - 1\right]; \qquad \text{(A23)}
\end{aligned}
$$

$$
\overline{H}_{AL4} = \alpha_s^2\alpha_{em}e_q^2C_F\frac{1+z^2}{1-z}\frac{1}{q_T^2}\frac{8(2\pi)^2}{N_c^2}\overline{I}_{L4}, \qquad \text{(A24)}
$$

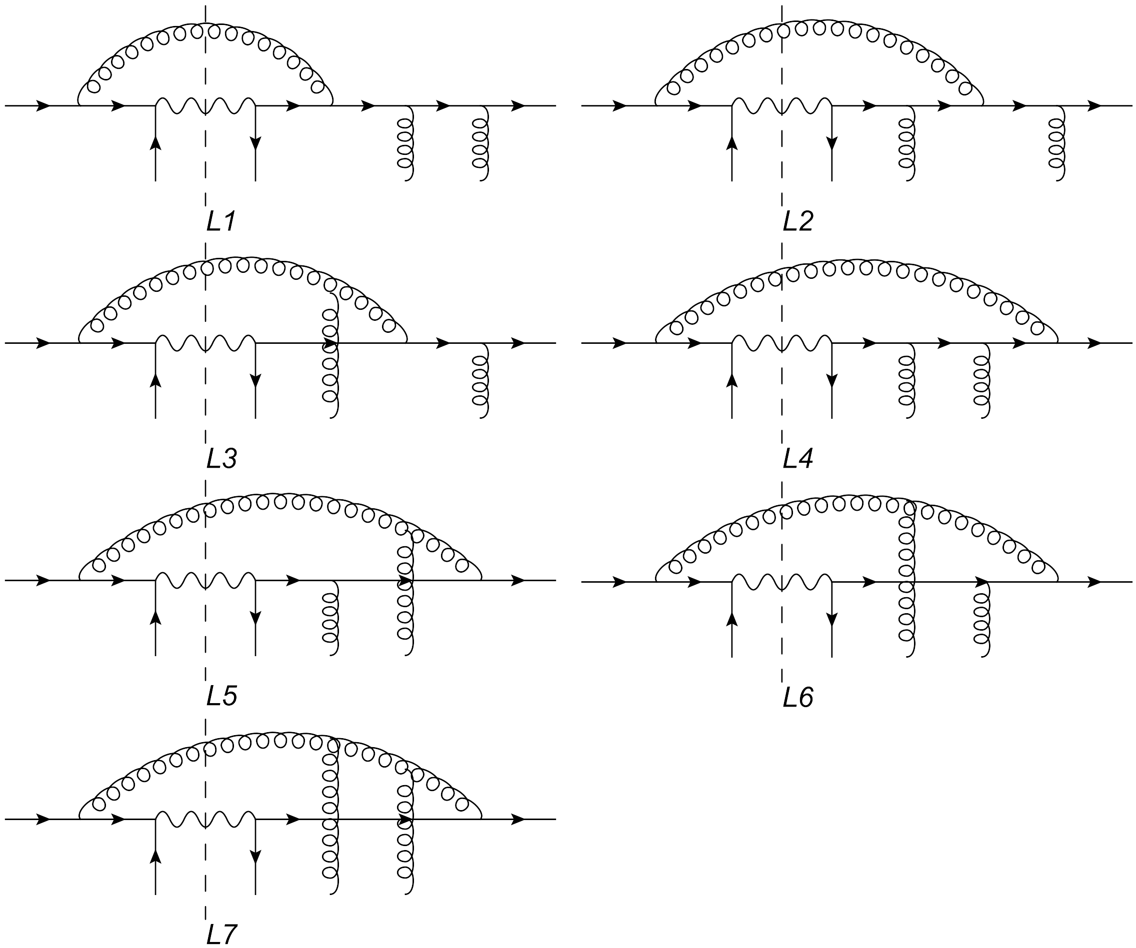

FIG. 11: Left-cut diagrams in annihilation-like process.

$$\overline{I}_{AL4} = -e^{i(x_B+x_t)p^+y^-}e^{i(x_E-x_t)p^+y_1^-}e^{-ix_Ep^+y_2^-}\theta(-y_2^-)\theta(y_2^- - y_1^-); \quad (A25)$$

$$\overline{H}_{AL5} = \alpha_s^2\alpha_{em}e_q^2\frac{C_A}{2}\frac{1+z^2}{1-z}\frac{q_T^2-\vec{k}_T\cdot\vec{q}_T}{(\vec{q}_T-\vec{k}_T)^2q_T^2}\frac{8(2\pi)^2}{N_c^2}\overline{I}_{L5}, \quad (A26)$$

$$\overline{I}_{AL5} = e^{i(x_B+x_t)p^+y^-}e^{i(x_E-x_t)p^+y_1^-}e^{-ix_Ep^+y_2^-}\theta(-y_2^-)\theta(y_2^- - y_1^-); \quad (A27)$$

$$\overline{H}_{AL6} = \alpha_s^2\alpha_{em}e_q^2\frac{C_A}{2}\frac{1+z^2}{1-z}\frac{q_T^2+\vec{k}_T\cdot\vec{q}_T}{q_T^2(\vec{q}_T+\vec{k}_T)^2}\frac{8(2\pi)^2}{N_c^2}\overline{I}_{L6}, \quad (A28)$$

$$\overline{I}_{AL6} = e^{i(x_B+x_t)p^+y^-}e^{-i(x_F+x_t)p^+y_1^-}e^{ix_Fp^+y_2^-}\theta(-y_2^-)\theta(y_2^- - y_1^-); \quad (A29)$$

$$\overline{H}_{AL7} = \alpha_s^2\alpha_{em}e_q^2C_A\frac{1+z^2}{1-z}\frac{1}{q_T^2}\frac{8(2\pi)^2}{N_c^2}\overline{I}_{L7}, \quad (A30)$$

$$\overline{I}_{AL7} = -e^{i(x_B+x_t)p^+y^-}e^{-i(x_F+x_t)p^+y_1^-}e^{ix_Fp^+y_2^-}\theta(-y_2^-)\theta(y_2^- - y_1^-). \quad (A31)$$

where,

$$x_E = \frac{x_B}{Q^2}(2\vec{q}_T\cdot\vec{k}_T - k_T^2), \quad x_F = \frac{x_B}{Q^2}\frac{z(k_T^2+2\vec{q}_T\cdot\vec{k}_T)}{1-z}. \quad (A32)$$

The right-cut diagrams are the complex conjugate of left-cut diagrams shown in Fig. 11,

their contributions are:

$$\overline{H}_{AR1} = \alpha_s^2\alpha_{em}e_q^2 C_F\frac{1+z^2}{1-z}\frac{1}{q_T^2}\frac{8(2\pi)^2}{N_c^2}\overline{I}_{R1}, \tag{A33}$$

$$\overline{I}_{AR1} = -e^{i(x_B+x_t)p^+y^-}e^{-ix_Dp^+(y_1^- - y_2^-)}\theta(y^- - y_1^-)\theta(y_1^- - y_2^-) \tag{A34}$$

$$\times \left[1 - e^{ix_tp^+(y_1^- - y_2^-)}e^{ix_tp^+(y_2^- - y^-)}\right]; \tag{A35}$$

$$\overline{H}_{AR2} = \alpha_s^2\alpha_{em}e_q^2\left(C_F - \frac{C_A}{2}\right)\frac{1+z^2}{1-z}\frac{q_T^2 - (1-z)\vec{k}_T\cdot\vec{q}_T}{q_T^2[\vec{q}_T - (1-z)\vec{k}_T]^2}\frac{8(2\pi)^2}{N_c^2}\overline{I}_{R2}, \tag{A36}$$

$$\overline{I}_{AR2} = e^{i(x_B+x_t)p^+y^-}e^{ix_Ep^+(y_1^- - y_2^-)}\theta(y^- - y_1^-)\theta(y_1^- - y_2^-);$$

$$\times e^{ix_tp^+(y_2^- - y^-)}\left[1 - e^{i(x_t - x_D - x_E)p^+(y_1^- - y_2^-)}\right]; \tag{A37}$$

$$\overline{H}_{AR3} = \alpha_s^2\alpha_{em}e_q^2\frac{C_A}{2}\frac{1+z^2}{1-z}\frac{q_T^2 + z\vec{k}_T\cdot\vec{q}_T}{q_T^2(\vec{q}_T + z\vec{k}_T)^2}\frac{8(2\pi)^2}{N_c^2}\overline{I}_{R3}, \tag{A38}$$

$$\overline{I}_{AR3} = e^{i(x_B+x_t)p^+y^-}e^{-ix_Fp^+(y_1^- - y_2^-)}\theta(y^- - y_1^-)\theta(y_1^- - y_2^-)$$

$$\times e^{ix_tp^+(y_2^- - y^-)}\left[1 - e^{i(x_t - x_D + x_F)p^+(y_1^- - y_2^-)}\right]; \tag{A39}$$

$$\overline{H}_{AR4} = \alpha_s^2\alpha_{em}e_q^2 C_F\frac{1+z^2}{1-z}\frac{1}{q_T^2}\frac{8(2\pi)^2}{N_c^2}\overline{I}_{R4}, \tag{A40}$$

$$\overline{I}_{AR4} = -e^{i(x_B+x_t)p^+y^-}e^{ix_Ep^+(y_1^- - y_2^-)}e^{ix_tp^+(y_2^- - y^-)}\theta(y^- - y_1^-)\theta(y_1^- - y_2^-); \tag{A41}$$

$$\overline{H}_{AR5} = \alpha_s^2\alpha_{em}e_q^2\frac{C_A}{2}\frac{1+z^2}{1-z}\frac{q_T^2 - \vec{k}_T\cdot\vec{q}_T}{(\vec{q}_T - \vec{k}_T)^2 q_T^2}\frac{8(2\pi)^2}{N_c^2}\overline{I}_{R5}, \tag{A42}$$

$$\overline{I}_{AR5} = e^{i(x_B+x_t)p^+y^-}e^{ix_Ep^+(y_1^- - y_2^-)}e^{ix_tp^+(y_2^- - y^-)}\theta(y^- - y_1^-)\theta(y_1^- - y_2^-); \tag{A43}$$

$$\overline{H}_{AR6} = \alpha_s^2\alpha_{em}e_q^2\frac{C_A}{2}\frac{1+z^2}{1-z}\frac{q_T^2 + \vec{k}_T\cdot\vec{q}_T}{q_T^2(\vec{q}_T + \vec{k}_T)^2}\frac{8(2\pi)^2}{N_c^2}\overline{I}_{R6}, \tag{A44}$$

$$\overline{I}_{AR6} = e^{i(x_B+x_t)p^+y^-}e^{-ix_Fp^+(y_1^- - y_2^-)}e^{ix_tp^+(y_2^- - y^-)}\theta(y^- - y_1^-)\theta(y_1^- - y_2^-); \tag{A45}$$

$$\overline{H}_{AR7} = \alpha_s^2\alpha_{em}e_q^2 C_A\frac{1+z^2}{1-z}\frac{1}{q_T^2}\frac{8(2\pi)^2}{N_c^2}\overline{I}_{R7}, \tag{A46}$$

$$\overline{I}_{AR7} = -e^{i(x_B+x_t)p^+y^-}e^{-ix_Fp^+(y_1^- - y_2^-)}e^{ix_tp^+(y_2^- - y^-)}\theta(y^- - y_1^-)\theta(y_1^- - y_2^-); \tag{A47}$$

Appendix B: complete results in Compton-like process

There are same amount of diagrams in Compton-like and annihilation-like processes, a total of 9 diagrams for central-cut, and 7 diagrams for left- and right-cut each. The central-cut diagrams are shown in Fig. 5 and their contributions are:

$$\overline{H}_{C11} = \alpha_s^2\alpha_{em}e_q^2\frac{C_A}{N_c^2-1}\frac{2z^2-2z+1}{(\vec{q}_T - z\vec{k}_T)^2}\frac{8(2\pi)^2}{N_c}\overline{I}_{C11}, \tag{B1}$$

$$\overline{H}_{C22} = \alpha_s^2\alpha_{em}e_q^2\frac{C_F}{N_c^2-1}\frac{2z^2-2z+1}{(\vec{q}_T - \vec{k}_T)^2}\frac{8(2\pi)^2}{N_c}\overline{I}_{C22}, \tag{B2}$$

$$\overline{H}_{C33} = \alpha_s^2\alpha_{em}e_q^2\frac{C_F}{N_c^2-1}\frac{2z^2-2z+1}{q_T^2}\frac{8(2\pi)^2}{N_c}\overline{I}_{C33}, \tag{B3}$$

$$\overline{H}_{C12} = \alpha_s^2\alpha_{em}e_q^2\frac{C_A}{2}\frac{1}{N_c^2-1}(2z^2-2z+1)\frac{[q_T^2-(1+z)\vec{k}_T\cdot\vec{q}_T+zk_T^2]}{(\vec{q}_T-\vec{k}_T)^2(\vec{q}_T-z\vec{k}_T)^2}\frac{8(2\pi)^2}{N_c}\overline{I}_{C12}, \tag{B4}$$

$$\overline{H}_{C13} = \alpha_s^2\alpha_{em}e_q^2\frac{C_A}{2}\frac{1}{N_c^2-1}(2z^2-2z+1)\frac{q_T^2-z\vec{k}_T\cdot\vec{q}_T}{q_T^2(\vec{q}_T-z\vec{k}_T)^2}\frac{8(2\pi)^2}{N_c}\overline{I}_{C13}, \tag{B5}$$

$$\overline{H}_{C21} = \alpha_s^2\alpha_{em}e_q^2\frac{C_A}{2}\frac{1}{N_c^2-1}(2z^2-2z+1)\frac{q_T^2-(1+z)\vec{k}_T\cdot\vec{q}_T+zk_T^2}{(\vec{q}_T-\vec{k}_T)^2(\vec{q}_T-z\vec{k}_T)^2}\frac{8(2\pi)^2}{N_c}\overline{I}_{C21}, \tag{B6}$$

$$\overline{H}_{C23} = \alpha_s^2\alpha_{em}e_q^2\left(C_F-\frac{C_A}{2}\right)\frac{1}{N_c^2-1}(2z^2-2z+1)\frac{q_T^2-\vec{k}_T\cdot\vec{q}_T}{q_T^2(\vec{q}_T-\vec{k}_T)^2}\frac{8(2\pi)^2}{N_c}\overline{I}_{C23}, \tag{B7}$$

$$\overline{H}_{C31} = \alpha_s^2\alpha_{em}e_q^2\frac{C_A}{2}\frac{1}{N_c^2-1}(2z^2-2z+1)\frac{q_T^2-z\vec{k}_T\cdot\vec{q}_T}{q_T^2(\vec{q}_T-z\vec{k}_T)^2}\frac{8(2\pi)^2}{N_c}\overline{I}_{C31}, \tag{B8}$$

$$\overline{H}_{C32} = \alpha_s^2\alpha_{em}e_q^2\left(C_F-\frac{C_A}{2}\right)\frac{1}{N_c^2-1}(2z^2-2z+1)\frac{q_T^2-\vec{k}_T\cdot\vec{q}_T}{q_T^2(\vec{q}_T-\vec{k}_T)^2}\frac{8(2\pi)^2}{N_c}\overline{I}_{C32}, \tag{B9}$$

and

$$\overline{I}_{Cij} = \overline{I}_{Aij}. \tag{B10}$$

The left-cut diagrams in Compton-like processes are shown in Fig. 12. Their contributions are:

$$\overline{H}_{CL1} = \alpha_s^2\alpha_{em}e_q^2\frac{C_A}{N_c^2-1}(2z^2-2z+1)\frac{1}{q_T^2}\frac{8(2\pi)^2}{N_c}\overline{I}_{L1}, \tag{B11}$$

$$\overline{I}_{CL1} = -e^{i(x_B+x_t)p^+y^-}e^{-ix_Dp^+(y_1^--y_2^-)}\left[1-e^{-ix_tp^+y_2^-}\right]\theta(-y_2^-)\theta(y_2^--y_1^-); \tag{B12}$$

$$\overline{H}_{CL2} = \alpha_s^2\alpha_{em}e_q^2\frac{C_A}{2(N_c^2-1)}(2z^2-2z+1)\frac{q_T^2-(1-z)\vec{k}_T\cdot\vec{q}_T}{q_T^2[\vec{q}_T-(1-z)\vec{k}_T]^2}\frac{8(2\pi)^2}{N_c}\overline{I}_{L2}, \tag{B13}$$

$$\begin{aligned}\overline{I}_{CL2} &= e^{i(x_B+x_t)p^+y^-}e^{-ix_Dp^+(y_1^--y_2^-)}\theta(-y_2^-)\theta(y_2^--y_1^-);\\ &\times e^{-ix_tp^+y_2^-}\left[e^{i(x_E-x_t+x_D)p^+(y_1^--y_2^-)}-1\right];\end{aligned} \tag{B14}$$

$$\overline{H}_{CL3} = \alpha_s^2\alpha_{em}e_q^2\frac{C_A}{2(N_c^2-1)}(2z^2-2z+1)\frac{q_T^2+z\vec{k}_T\cdot\vec{q}_T}{q_T^2(\vec{q}_T+z\vec{k}_T)^2}\frac{8(2\pi)^2}{N_c}\overline{I}_{L3}, \tag{B15}$$

$$\begin{aligned}\overline{I}_{CL3} &= e^{i(x_B+x_t)p^+y^-}e^{-ix_Dp^+(y_1^--y_2^-)}\theta(-y_2^-)\theta(y_2^--y_1^-)\\ &\times e^{-ix_tp^+y_2^-}\left[e^{i(-x_F-x_t+x_D)p^+(y_1^--y_2^-)}-1\right];\end{aligned} \tag{B16}$$

$$\overline{H}_{CL4} = \alpha_s^2\alpha_{em}e_q^2\frac{C_F}{N_c^2-1}(2z^2-2z+1)\frac{1}{q_T^2}\frac{8(2\pi)^2}{N_c}\overline{I}_{L4}, \tag{B17}$$

$$\overline{I}_{CL4} = -e^{i(x_B+x_t)p^+y^-}e^{i(x_E-x_t)p^+y_1^-}e^{-ix_Ep^+y_2^-}\theta(-y_2^-)\theta(y_2^--y_1^-); \tag{B18}$$

$$\overline{H}_{CL5} = \alpha_s^2\alpha_{em}e_q^2\frac{C_F-C_A/2}{N_c^2-1}(2z^2-2z+1)\frac{q_T^2-\vec{k}_T\cdot\vec{q}_T}{(\vec{q}_T-\vec{k}_T)^2q_T^2}\frac{8(2\pi)^2}{N_c}\overline{I}_{L5}, \tag{B19}$$

$$\overline{I}_{CL5} = e^{i(x_B+x_t)p^+y^-}e^{i(x_E-x_t)p^+y_1^-}e^{-ix_Ep^+y_2^-}\theta(-y_2^-)\theta(y_2^--y_1^-); \tag{B20}$$

$$\overline{H}_{CL6} = \alpha_s^2\alpha_{em}e_q^2\frac{C_F-C_A/2}{N_c^2-1}(2z^2-2z+1)\frac{q_T^2+\vec{k}_T\cdot\vec{q}_T}{q_T^2(\vec{q}_T+\vec{k}_T)^2}\frac{8(2\pi)^2}{N_c}\overline{I}_{L6}, \tag{B21}$$

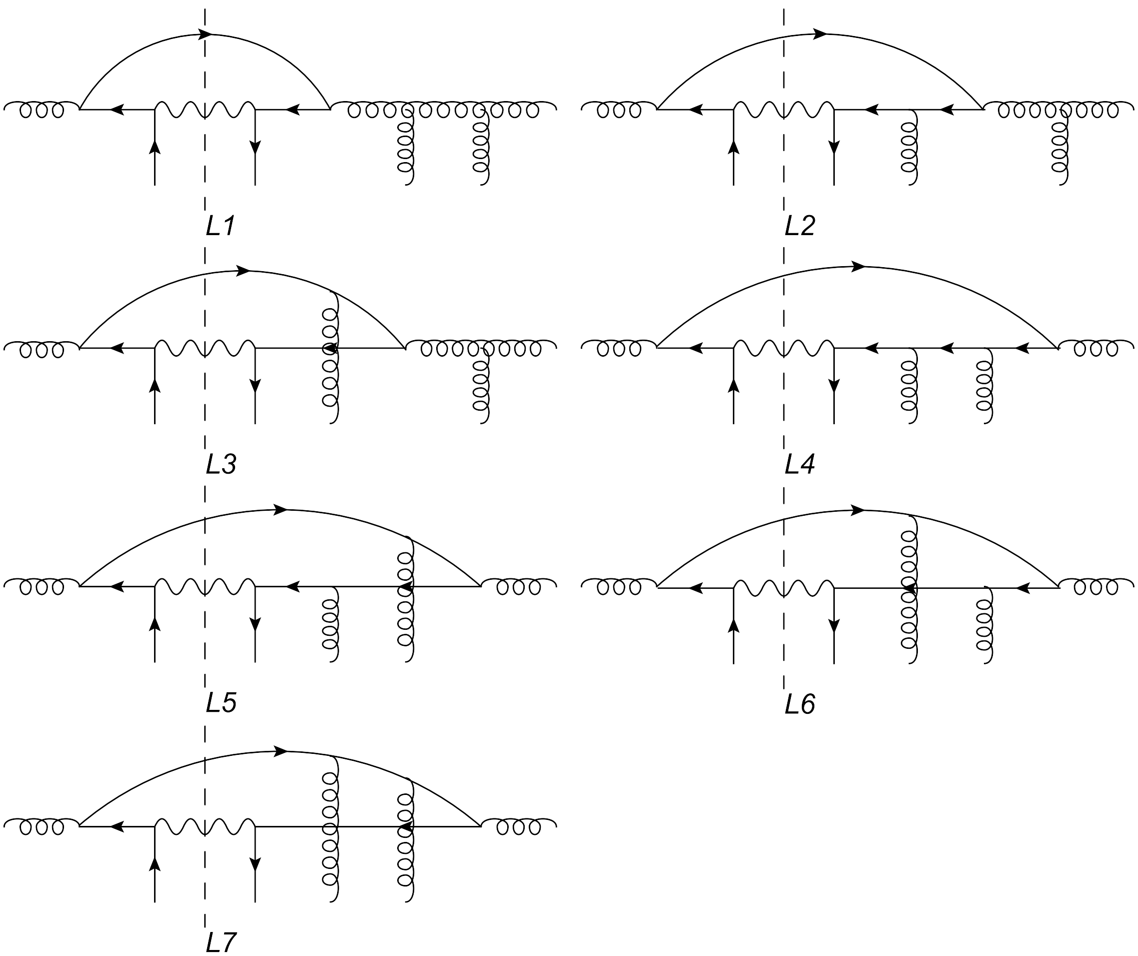

FIG. 12: Left-cut diagrams in compton-like process.

$$\overline{I}_{CL6} = e^{i(x_B+x_t)p^+y^-}e^{-i(x_F+x_t)p^+y_1^-}e^{ix_Fp^+y_2^-}\theta(-y_2^-)\theta(y_2^- - y_1^-); \tag{B22}$$

$$\overline{H}_{CL7} = \alpha_s^2\alpha_{em}e_q^2\frac{C_F}{N_c^2-1}(2z^2-2z+1)\frac{1}{q_T^2}\frac{8(2\pi)^2}{N_c}\overline{I}_{L7}, \tag{B23}$$

$$\overline{I}_{CL7} = -e^{i(x_B+x_t)p^+y^-}e^{-i(x_F+x_t)p^+y_1^-}e^{ix_Fp^+y_2^-}\theta(-y_2^-)\theta(y_2^- - y_1^-). \tag{B24}$$

The right-cut diagrams are the complex conjugate of left-cut diagrams shown in Fig. 12 and the results are:

$$\overline{H}_{CR1} = \alpha_s^2\alpha_{em}e_q^2\frac{C_A}{N_c^2-1}(2z^2-2z+1)\frac{1}{q_T^2}\frac{8(2\pi)^2}{N_c}\overline{I}_{R1}, \tag{B25}$$

$$\overline{I}_{CR1} = -e^{i(x_B+x_t)p^+y^-}e^{-ix_Dp^+(y_1^- - y_2^-)}\theta(y^- - y_1^-)\theta(y_1^- - y_2^-) \tag{B26}$$

$$\times \left[1 - e^{ix_tp^+(y_1^- - y_2^-)}e^{ix_tp^+(y_2^- - y^-)}\right]; \tag{B27}$$

$$\overline{H}_{CR2} = \alpha_s^2\alpha_{em}e_q^2\frac{C_A}{2(N_c^2-1)}(2z^2-2z+1)\frac{q_T^2-(1-z)\vec{k}_T\cdot\vec{q}_T}{q_T^2[\vec{q}_T-(1-z)\vec{k}_T]^2}\frac{8(2\pi)^2}{N_c}\overline{I}_{R2}, \tag{B28}$$

$$\overline{I}_{CR2} = e^{i(x_B+x_t)p^+y^-}e^{ix_Ep^+(y_1^- - y_2^-)}\theta(y^- - y_1^-)\theta(y_1^- - y_2^-);$$

$$\times\ e^{ix_tp^+(y_2^- - y^-)}\left[1 - e^{i(x_t-x_D-x_E)p^+(y_1^- - y_2^-)}\right]; \tag{B29}$$

$$\overline{H}_{CR3} = \alpha_s^2\alpha_{em}e_q^2\frac{C_A}{2(N_c^2-1)}(2z^2-2z+1)\frac{q_T^2+z\vec{k}_T\cdot\vec{q}_T}{q_T^2(\vec{q}_T+z\vec{k}_T)^2}\frac{8(2\pi)^2}{N_c}\overline{I}_{R3}, \tag{B30}$$

$$\begin{aligned}\overline{I}_{CR3} &= e^{i(x_B+x_t)p^+y^-}e^{-ix_Fp^+(y_1^--y_2^-)}\theta(y^--y_1^-)\theta(y_1^--y_2^-) \\ &\times e^{ix_tp^+(y_2^--y^-)}\left[1-e^{i(x_t-x_D+x_F)p^+(y_1^--y_2^-)}\right];\end{aligned} \tag{B31}$$

$$\overline{H}_{CR4} = \alpha_s^2\alpha_{em}e_q^2\frac{C_F}{N_c^2-1}(2z^2-2z+1)\frac{1}{q_T^2}\frac{8(2\pi)^2}{N_c}\overline{I}_{R4}, \tag{B32}$$

$$\overline{I}_{CR4} = -e^{i(x_B+x_t)p^+y^-}e^{ix_Ep^+(y_1^--y_2^-)}e^{ix_tp^+(y_2^--y^-)}\theta(y^--y_1^-)\theta(y_1^--y_2^-); \tag{B33}$$

$$\overline{H}_{CR5} = \alpha_s^2\alpha_{em}e_q^2\frac{C_F-C_A/2}{N_c^2-1}(2z^2-2z+1)\frac{q_T^2-\vec{k}_T\cdot\vec{q}_T}{(\vec{q}_T-\vec{k}_T)^2q_T^2}\frac{8(2\pi)^2}{N_c}\overline{I}_{R5}, \tag{B34}$$

$$\overline{I}_{CR5} = e^{i(x_B+x_t)p^+y^-}e^{ix_Ep^+(y_1^--y_2^-)}e^{ix_tp^+(y_2^--y^-)}\theta(y^--y_1^-)\theta(y_1^--y_2^-); \tag{B35}$$

$$\overline{H}_{CR6} = \alpha_s^2\alpha_{em}e_q^2\frac{C_F-C_A/2}{N_c^2-1}(2z^2-2z+1)\frac{q_T^2+\vec{k}_T\cdot\vec{q}_T}{q_T^2(\vec{q}_T+\vec{k}_T)^2}\frac{8(2\pi)^2}{N_c}\overline{I}_{R6}, \tag{B36}$$

$$\overline{I}_{CR6} = e^{i(x_B+x_t)p^+y^-}e^{-ix_Fp^+(y_1^--y_2^-)}e^{ix_tp^+(y_2^--y^-)}\theta(y^--y_1^-)\theta(y_1^--y_2^-); \tag{B37}$$

$$\overline{H}_{CR7} = \alpha_s^2\alpha_{em}e_q^2\frac{C_F}{N_c^2-1}(2z^2-2z+1)\frac{1}{q_T^2}\frac{8(2\pi)^2}{N_c}\overline{I}_{R7}, \tag{B38}$$

$$\overline{I}_{CR7} = -e^{i(x_B+x_t)p^+y^-}e^{-ix_Fp^+(y_1^--y_2^-)}e^{ix_tp^+(y_2^--y^-)}\theta(y^--y_1^-)\theta(y_1^--y_2^-); \tag{B39}$$

Appendix C: Cross-check of double hard processes

One can extract the double-hard subprocesses in annihilation-like and Compton-like process from Eq. (26) and Eq. (36),

$$\begin{aligned}\frac{d\sigma^{AHH}_{hA\to\gamma^*}}{dQ^2dx'} &= \sum_q\int dxH_0(x,p,q)\int_0^{\mu^2}\frac{dq_T^2}{q_T^4}\frac{\alpha_s}{2\pi}\int_{x'}^1\frac{d\xi}{\xi}f_{q/h}(\xi)\frac{1+z^2}{1-z}\frac{2\pi\alpha_s}{N_c} \\ &\times \left[C_Az+C_F(1-z)^2\right]T_{HH}(x,x_t),\end{aligned} \tag{C1}$$

$$\begin{aligned}\frac{d\sigma^{CHH}_{hA\to\gamma^*}}{dQ^2dx'} &= \sum_q\int dxH_0(x,p,q)\int_0^{\mu^2}\frac{dq_T^2}{q_T^4}\frac{\alpha_s}{2\pi}\int_{x'}^1\frac{d\xi}{\xi}f_{g/h}(\xi)\left[z^2+(1-z)^2\right]\frac{2\pi\alpha_s}{N_c^2-1} \\ &\times \left[C_F-C_Az(1-z)\right]T_{HH}(x,x_t),\end{aligned} \tag{C2}$$

where,

$$\begin{aligned}T_{HH}(x,x_t) &= \int\frac{dy^-}{2\pi}dy_1^-dy_2^-e^{ixp^+y^-}e^{ix_tp^+(y_1^--y_2^-)} \\ &\times \frac{1}{2}\langle A|F_\alpha^+(y_2^-)\bar{\psi}_q(0)\gamma^+\psi_q(y^-)F^{+\alpha}(y_1^-)|A\rangle\theta(-y_2^-)\theta(y^--y_1^-) \\ &\approx \pi\int dy_N^-\rho_A(y_N)f_{q/A}(x)x_tf_{g/N}(x_t)\end{aligned} \tag{C3}$$

with $\rho_A(y_N)$ being the nucleon density distribution. A factorized form of gluon-quark correlation is assumed in the above equation. With this assumption, one can factorized the

double-hard subprocess as,

$$\begin{aligned}
\frac{d\sigma^{AHH}_{hA\to\gamma^*}}{dQ^2} &= \sum_q \int dx d\xi H_0(x,p,q) f_{q/h}(\xi) f_{\bar{q}/A}(x) \int dy_N^- \rho_A(y_N) \\
&\times \pi\alpha_s^2 x_t f_{g/N}(x_t) \frac{1+z^2}{1-z}\left[\frac{C_A}{N_c} z + \frac{C_F}{N_c}(1-z)^2\right] dz \frac{dq_T^2}{q_T^4} \\
&\equiv \frac{d\sigma^{S(0)}_{hA\to l^+l^-}}{dQ^2} \int dy_N^- \rho_A(y_N) d\sigma_{qN}, \qquad \text{(C4)} \\
\frac{d\sigma^{CHH}_{hA\to\gamma^*}}{dQ^2} &= \sum_q \int dx d\xi H_0(x,p,q) f_{g/h}(\xi) f_{q/A}(x) \int dy_N^- \rho_A(y_N) \\
&\times \pi\alpha_s^2 x_t f_{g/N}(x_t) \left[z^2 + (1-z)^2\right] \left[\frac{C_F}{N_c^2-1} - \frac{C_A}{N_c^2-1} z(1-z)\right] dz \frac{dq_T^2}{q_T^4} \\
&\equiv \frac{d\sigma^{S(0)}_{hA\to l^+l^-}}{dQ^2} \int dy_N^- \rho_A(y_N) d\sigma_{gN}. \qquad \text{(C5)}
\end{aligned}$$

Here $d\sigma^{S(0)}_{hA\to\gamma^*}/dQ^2$ is the Born cross section defined in Eq. (6). $d\sigma_{qN}$ and $d\sigma_{gN}$ represent the cross section of the parton-nucleon scattering. Since the gluon is physical and has finite momentum fraction $x_t p^+$ in the double-hard process, the higher-twist results have simple and intuitive partonic interpretation as stated in the above equations. This comes from the assumption that the twist-4 contributions from double scattering can be factorized into two successive and isolated single scatterings. In the following, we rederive the twist-4 contributions from double-hard scattering based on the above assumption [49].

Consider the parton-nucleon scattering

$$a(p') + N(p) \to c(q) + d(k) + X \qquad \text{(C6)}$$

where,

$$p' = [0, p'^-, 0], \qquad p = [p^+, 0, 0], \qquad q = \left[\frac{q_T^2}{2zp'^-}, zp'^-, \vec{q}_T\right]. \qquad \text{(C7)}$$

The parton nucleon cross section can be written as

$$\begin{aligned}
d\sigma_{aN} &= \int d\sigma_{ag} f_{g/N}(x) dx \qquad \text{(C8)} \\
&= \int dx f_{g/N}(x) \frac{g^4}{2s} |M|^2_{ag\to cd}(s,t,u) \frac{d^3q}{(2\pi)^3 2q_0} 2\pi\delta[(p'+xp-q)^2] \qquad \text{(C9)} \\
&= \frac{g^4}{(4\pi)^2} x_t f_{g/N}(x_t) |M|^2_{ag\to cd}(s,t,u) \frac{\pi}{s^2} \frac{dz}{z(1-z)} dq_T^2, \qquad \text{(C10)}
\end{aligned}$$

where $x_t = q_T^2/[2p\cdot q(1-z)]$ because of the on-shell condition of the final parton. The Mandelstam variables in this partonic process can be recast as

$$s = (p'+xp)^2 = \frac{q_T^2}{z(1-z)}, \quad t = (q-p')^2 = -\frac{q_T^2}{z}, \quad u = (q-xp)^2 = -\frac{q_T^2}{1-z}. \qquad \text{(C11)}$$

In the annihilation-like and Compton-like double scattering processes, the first hard scattering is the quark-gluon Compton scattering and gluon-gluon fusion, respectively. The partonic matrix element for these two processes are

$$\begin{aligned}
|M|^2_{qg\to qg}(s,t,u) &= \frac{C_A}{N_c}\frac{s^2+u^2}{t^2} - \frac{C_F}{N_c}\frac{s^2+u^2}{us} \\
&= \frac{C_A}{N_c}\frac{1+z^2}{(1-z)^2} + \frac{C_F}{N_c}\frac{1+z^2}{z} \qquad \text{(C12)}\\
|M|^2_{gg\to q\bar{q}}(s,t,u) &= \frac{C_F}{N_c^2-1}\frac{t^2+u^2}{tu} - \frac{C_A}{N_c^2-1}\frac{t^2+u^2}{s^2} \\
&= \frac{C_F}{N_c^2-1}\frac{z^2+(1-z)^2}{z(1-z)} - \frac{C_A}{N_c^2-1}[z^2+(1-z)^2]. \qquad \text{(C13)}
\end{aligned}$$

Substituting the above equations into Eq. (C8), one can obtain the quark-nucleon and gluon-nucleon cross section,

$$\begin{aligned}
d\sigma_{qN} &= \pi\alpha_s^2 x_t f_{g/N}(x_t)\left[\frac{C_A}{N_c}z + \frac{C_F}{N_c}(1-z)^2\right]\frac{1+z^2}{1-z}dz\frac{dq_T^2}{q_T^4}, \qquad \text{(C14)}\\
d\sigma_{gN} &= \pi\alpha_s^2 x_t f_{g/N}(x_t)\left[\frac{C_F}{N_c^2-1} - \frac{C_A}{N_c^2-1}z(1-z)\right]\left[z^2+(1-z)^2\right]dz\frac{dq_T^2}{q_T^4}, \qquad \text{(C15)}
\end{aligned}$$

which are equivalent to the results in Eq. (C4) and Eq. (C5).

---

[1] R. K. Ellis, W. Furmanski, R. Petronzio, Nucl. Phys. **B207**, 1 (1982); **B212**, 29 (1983).

[2] J. -W. Qiu, G. F. Sterman, Nucl. Phys. **B353**, 105-136 (1991); **B353**, 137-164 (1991).

[3] M. Luo, J. -W. Qiu, G. F. Sterman, Phys. Lett. **B279**, 377-383 (1992); Phys. Rev. **D49**, 4493-4502 (1994); **D50**, 1951-1971 (1994).

[4] J. Osborne and X. -N. Wang, Nucl. Phys. **A710**, 281 (2002).

[5] J. C. Solana, X. -N. Wang, Phys. Rev. **C77**, 024902 (2008).

[6] A. Airapetian *et al.* [HERMES Collaboration], Eur. Phys. J. **C20**, 479 (2001); V. Muccifora [HERMES Collaboration], Nucl. Phys. **A715**, 506 (2003); A. Airapetian *et al.* [HERMES Collaboration], Nucl. Phys. **B780**, 1 (2007).

[7] X. -F. Guo, X. -N. Wang, Phys. Rev. Lett. **85**, 3591-3594 (2000); X. -N. Wang, X. -F. Guo, Nucl. Phys. **A696**, 788-832 (2001).

[8] B. -W. Zhang, X. -N. Wang, Nucl. Phys. **A720**, 429-451 (2003).

[9] A. Majumder, E. Wang, X. -N. Wang, Phys. Rev. Lett. **99**, 152301 (2007). [nucl-th/0412061].

[10] A. Majumder, B. Muller, Phys. Rev. **C77**, 054903 (2008). [arXiv:0705.1147 [nucl-th]].

[11] Z. -T. Liang, X. -N. Wang, J. Zhou, Phys. Rev. **D77**, 125010 (2008).

[12] L. D. McLerran and R. Venugopalan, Phys. Rev. **D49**, 2233 (1994).

[13] Y. V. Kovchegov, A. H. Mueller, Nucl. Phys. **B529**, 451-479 (1998).

[14] E. Wang, X. -N. Wang, Phys. Rev. Lett. **89**, 162301 (2002).

[15] W. -T. Deng, X. -N. Wang, Phys. Rev. **C81**, 024902 (2010).

[16] A. Majumder, C. Nonaka, S. A. Bass, Phys. Rev. **C76**, 041902 (2007). [nucl-th/0703019].

[17] M. Gyulassy and M. Plumer, Phys. Lett. **B243**, 432 (1990); X. -N. Wang and M. Gyulassy, Phys. Rev. Lett. **68**, 1480 (1992).

[18] C. Adler *et al* [STAR Collaboration], Phys. Rev. Lett. **89**, 202301 (2002).
[19] K. Adcox *et al* [PHENIX Collaboration], Phys. Rev. Lett. **88**, 022301 (2002).
[20] C. Adler *et al* [STAR Collaboration], Phys. Rev. Lett. **90**, 082302 (2003).
[21] A. Adare *et al.* [PHENIX Collaboration], Phys. Rev. **C80**, 024908 (2009).
[22] B. I. Abelev *et al.* [STAR Collaboration], Phys. Rev. **C82**, 034909 (2010).
[23] M. Gyulassy and L. McLerran, Nucl. Phys. **A750**, 30 (2005).
[24] P. Jacobs and X. -N. Wang, Prog. Part. Nucl. Phys. **54**, 443 (2005).
[25] Proceedings of Quark Matter 2011, 23-28 May 2011, Annecy, France.
[26] M. Gyulassy and X. -N. Wang, Nucl. Phys. **B420**, 583 (1994); X. -N. Wang, M. Gyulassy and M. Plumer, Phys. Rev. **D51**, 3436 (1995).
[27] R. Baier, Yu. L. Dokshitzer, S. Peigne and D. Schiff, Phys. Lett. **B345**, 277 (1995); R. Baier, Yu. L. Dokshitzer, A. Mueller, S. Peigne and D. Schiff, Nucl. Phys. **B484**, 265 (1997).
[28] B. G. Zhakharov, JETP letters **63**, 952 (1996); *ibid.* 65, 615(1997).
[29] M. Gyulassy, P. Levai and I. Vitev, Nucl. Phys. **B594**, 371 (2001); Phys. Rev. Lett. **85**, 5535 (2000).
[30] X. F. Chen, *et al*, Phys. Rev. **C81**, 064908 (2010); X. F. Chen, *et al*, arxiv: 1102.5614.
[31] S. Gavin, J. Milana, Phys. Rev. Lett. **68**, 1834-1837 (1992).
[32] M. A. Vasilev *et al.* [FNAL E866 Collaboration], Phys. Rev. Lett. **83**, 2304 (1999).
[33] M. B. Johnson, B. Z. Kopeliovich, I. K. Potashnikova, P. L. McGaughey, J. M. Moss, J. C. Peng, G. Garvey, M. Leitch *et al.*, Phys. Rev. **C65**, 025203 (2002).
[34] F. Arleo, Phys. Lett. **B532**, 231-239 (2002).
[35] G. T. Garvey, J. C. Peng, Phys. Rev. Lett. **90**, 092302 (2003).
[36] C. G. Duan, N. Liu, G. L. Li, Phys. Rev. **C79**, 048201 (2009).
[37] I. Vitev, Phys. Rev. **C75**, 064906 (2007), arXiv:hep-ph/0703002; R. B. Neufeld, I. Vitev and B. W. Zhang, Phy. Lett. **B704** 590 (2011), arXiv:1010.3708.
[38] X. F. Guo, Phys. Rev. **D58**, 036001 (1998).
[39] R. J. Fries, B. Muller, A. Schafer and E. Stein, Phys. Rev. Lett. **83**, 4261 (1999); R. J. Fries, A. Schafer, E. Stein and B. Muller, Nucl. Phys. **B582**, 537 (2000).
[40] L. D. Landau and I. J. Pomeranchuk, Dolk. Akad. Nauk. SSSR **92**, 92(1953); A. B. Migdal, Phys. Rev. **103**, 1811(1956).
[41] In a very narrow region where the momentum fraction carried by the beam parton is very close to zero, there exists a small enhancement effect due to the momentum sum rule of the parton distribution function. We will ignore this region in this paper because the lack of experimental data in this region.
[42] J. Ashman *et al.* [European Muon Collaboration], Z. Phys. **C57**, 211 (1993).
[43] K. J. Eskola, H. Paukkunen, C. A. Salgado. JHEP **0807**, 102 (2008).
[44] M. Hirai, S. Kumano, T. -H. Nagai, Phys. Rev. **C76**, 065207 (2007). [arXiv:0709.3038 [hep-ph]].
[45] V. N. Gribov, L. N. Lipatov, Sov. J. Nucl. Phys. **15**, 438-450 (1972); Y. L. Dokshitzer, Sov. Phys. JETP **46**, 641-653 (1977).
[46] G. Altarelli, G. Parisi, Nucl. Phys. **B126**, 298 (1977).
[47] J. C. Collins, D. E. Soper and G. Sterman, in *Perturbative Quantum Chromodynamics*, edited by A. H. Muller (World Scientific, Singapore, 1989).
[48] S. D. Drell and T. M. Yan, Phys. Rev. Lett. **25**, 316 (1970); Ann. Phys. (N. Y.) **66**, 578 (1971).
[49] A. Schafer, B. -W. Zhang and X. -N. Wang, Nucl. Phys. **A793**, 128 (2007).

[50] J. -W. Qiu, Phys. Rev. **D42**, 30 (1990).
[51] X. -F. Guo, Phys. Rev. **D58**, 114033 (1998).
[52] A. H. Mueller and J. -W. Qiu, Nucl. Phys. **B268**, 427 (1986).
[53] J. Pumplin *et al.* JHEP **0207**, 012 (2002).
[54] P. E. Reimer, J. Phys. **G34**, S107 (2007).
[55] E906 home page: http://www.phy.anl.gov/mep/SeaQuest/